

**APPLICATION OF NUMERICAL MODEL CGWAVE FOR WAVE
PREDICTION AT PONCE DE LEON INLET, FLORIDA, USA**

By

Nishchey Chhabra

A.S. Dayananda Sagar Institute of Technology, 1993

B.S. University of Maine, 1996

A THESIS

Submitted in Partial Fulfillment of the
Requirements for the Degree of
Master of Science
(in Mechanical Engineering)

The Graduate School
The University of Maine

May, 2004

Advisory Committee:

Vijay G. Panchang, Professor & Head, Maritime Systems Engineering, Texas
A&M University – Galveston, Advisor

Michael Boyle, Associate Professor of Mechanical Engineering

Justin Poland, Associate Professor of Mechanical Engineering

Zeki Demirbilek, Researcher, US Army R&D Center, Coastal & Hydraulics
Laboratory, Vicksburg, MS

**APPLICATION OF NUMERICAL MODEL CGWAVE FOR WAVE
PREDICTION AT PONCE DE LEON INLET, FLORIDA, USA**

By Nishchey Chhabra

Thesis Advisor: Dr. Vijay G. Panchang

An Abstract of the Thesis Presented
in Partial Fulfillment of the Requirements for the
Degree of Master of Science
(in Mechanical Engineering)
May, 2004

This thesis describes the use of the numerical model CGWAVE to predict wave conditions at Ponce de Leon Inlet, Florida. Model predictions are compared to measured wave heights obtained from a physical model study conducted at the Army Corps of Engineers Waterways Experiment Station (WES). CGWAVE is a state-of-the-art coastal surface water wave prediction model based on the mild slope equation, which may be used to predict waves in design studies for ports and harbors, open coasts, inlets, around islands, and estuaries. Ports and harbors are used for commercial, recreational and military purposes. Waterborne commerce has significant advantages over other kinds of transportation means due to its low cost and high capacity. Several major U.S. ports/harbors currently have renovations plans in response to the future expansion of ocean-borne world commerce, and related engineering projects generally require a detailed knowledge of the wave field in the project areas. Physical and numerical model studies are often conducted concurrently for these projects to evaluate technical feasibility and to optimize design alternatives. The Army Corps of Engineers Waterways

Experiment Station (WES) constructed a 1:100 scale physical model of Ponce de Leon Inlet, Florida and utilized it for studying the transformation of waves for evaluation of their models and the project needs. The physical model study used both monochromatic and spectral wave conditions that covered a wide range of wave periods and wave directions. Wave heights recorded by twelve gauges were used in this research to determine how well the CGWAVE model could reproduce the measurements. This model validation study can be used to guide future applications of CGWAVE in other projects. Lessons learned and knowledge gained about model performance can help users to determine the applicability of this model and thus may help to reduce the need for field or laboratory data measurements that may be costly. The performance of the numerical model CGWAVE in Ponce Inlet is described in this thesis, and model estimates are compared to measured data.

ACKNOWLEDGEMENTS

This research was supported by the Office of Naval Research, the Maine Sea Grant Program, and the Army Corps of Engineers. I am greatly appreciative of their support.

I wish to thank Professor Vijay Panchang for his time, effort and guidance throughout the course of my study. I also wish to thank Dr. Zeki Demirebilek for having made valuable suggestions and helped running the simulations. In addition, I would like to thank Professor Justin Poland and Professor Michael Boyle for their contributions.

Special thanks are extended to Mr. Karl Schlenker, for his continuous assistance in the use of SMS and to Mr. Liuzhi Zhao for continuing the research work on Ponce De Leon Inlet, Florida. I also would like to thank my wife and parents for their love and emotional support throughout my studies at University of Maine and in the completion of this thesis.

TABLE OF CONTENTS

ACKNOWLEDGEMENTS.....	ii
LIST OF TABLES.....	v
LIST OF FIGURES.....	vi
Chapter	
1. INTRODUCTION.....	1
2. PHYSICAL MODEL PONCE DE LEON INLET.....	6
2.1. Summary of Physical Model Study.....	6
2.2. Characteristics of Measured Data.....	7
3. THE NUMERICAL MODEL CGWAVE.....	15
3.1. Background.....	15
3.2. Model Description.....	16
3.3. Fundamental Equations.....	16
3.4. Treatment of Boundary Conditions.....	19
3.4.1. Land (Closed) Boundary Conditions.....	20
3.4.2. Open Boundary Conditions.....	21
3.5. Numerical Solution Scheme.....	23
3.6. Wave Breaking Schemes.....	25

- 4. GRID GENERATION FOR CGWAVE USING SURFACE-WATER MODELING SYSTEM (SMS).....27
 - 4.1. Overview of SMS.....27
 - 4.2. Numerical Model Grid Generation Using SMS.....28
 - 4.3. Creating Spectral Components.....30
- 5. NUMERICAL PREDICTIONS.....38
 - 5.1. Monochromatic Wave Results.....38
 - 5.2. Spectral Simulations.....49
- 6. SUMMARY AND CONCLUSIONS.....59
- REFERENCES.....65
- BIOGRAPHY OF THE AUTHOR.....70

LIST OF TABLES

Table 1.	Monochromatic and Spectral Input Wave Conditions (Reference).....	11
Table 2.	Resolution analysis for wave period 15 sec.....	31
Table 3.	Resolution analysis for wave period 10 sec.....	32
Table 4.	Resolution analysis for wave period 8 sec.....	33
Table 5.	Summary of input and boundary conditions - for monochromatic cases.....	42
Table 6.	RMS wave height errors for Transect 1 monochromatic cases.....	47
Table 7.	RMS wave height errors for Transect 2 monochromatic cases.....	48
Table 8.	Input conditions for spectral simulations for spectral cases.....	51
Table 9.	Boundary conditions for spectral simulations for spectral cases.....	52
Table 10.	RMS wave height errors for Transect 1 spectral cases	55
Table 11.	RMS wave height errors for Transect 2 spectral cases.....	56

LIST OF FIGURES

Figure 1.	Physical model of Ponce Inlet (Reference).....	4
Figure 2.	Contours and orientation of numerical model Ponce de Leon Inlet.....	12
Figure 3.	Contours and features of numerical model Ponce de Leon Inlet.....	13
Figure 4.	Wave model domain definition sketch.....	22
Figure 5.	Spectral Energy Density for 18 frequency components.....	36
Figure 6.	Directional Spectra curve for 17 directional bins.....	36
Figure 7.	Estimated wave heights for Ponce de Leon Inlet from SMS.....	40
Figure 8.	Estimated wave phase diagram for Ponce de Leon Inlet from SMS.....	41
Figure 9.	Wave height for Transect 1 monochromatic case 1.....	45
Figure 10.	Wave height for Transect 1 monochromatic case 2.....	45
Figure 11.	Wave height for Transect 1 monochromatic case 3.....	45
Figure 12.	Wave height for Transect 2 monochromatic case 1.....	46
Figure 13.	Wave height for Transect 2 monochromatic case 2.....	46
Figure 14.	Wave height for Transect 2 monochromatic case 3.....	46
Figure 15.	Wave height for Transect 1 spectral case 1 (case # 4 in Table 1).....	53
Figure 16.	Wave height for Transect 1 spectral case 2 (case # 5 in Table 1).....	53
Figure 17.	Wave height for Transect 1 spectral case 3 (case # 6 in Table 1).....	53
Figure 18.	Wave height for Transect 2 spectral case 1 (case # 4 in Table 1).....	54
Figure 19.	Wave height for Transect 2 spectral case 2 (case # 5 in Table 1).....	54
Figure 20.	Wave height for Transect 2 spectral case 3 (case # 6 in Table 1).....	54

Chapter 1

INTRODUCTION

Waves play a significant role in all ocean-related activities. They damage shore protection structures, reshape beaches and affect moored vessels in inadequately protected ports and harbors which are usually centers of waterborne transportation and are hence important for commercial, military, and recreational activities. For instance, about \$600 billion in foreign trade passed through ports in the United States in 1997; this trade is projected to triple by 2020 (YOTO, 1998). Engineers must provide the infrastructure that can handle this growth. Harbor facilities must accommodate ever-larger ships (“megaships”) with increasingly demanding schedules and complex environmental regulations. It is necessary that these facilities be designed in a manner that enhances efficiency and safety of harbor operations such as cargo loading/unloading etc. Therefore, it becomes necessary to understand the characteristics of waves that impact various operations in ports and harbors. However, in most cases, little (if any) wave data are available for engineering construction and planning. Field observation and physical modeling of waves are extremely difficult, costly and time-consuming. Remote-sensing instruments, used in recent years, do not systematically provide the desired resolution in the near shore region and no data-recording instrument can in any case anticipate future sea states. The desired sea-state information may thus be obtained and project plans evaluated with reliable numerical wave models.

CGWAVE is an efficient and easy-to-use wave prediction numerical model. The model can provide the base information pertaining to shallow water wave propagation and transformation in harbor/coastal projects or offshore open sea problems. The wave prediction model CGWAVE was developed at the University of Maine, in collaboration with the Army Corps of Engineers, with additional funding from the US Navy and the National Sea Grant Program. The model is applicable to studies of waves in harbors, open coastal regions, around islands in areas of arbitrary geometry. While CGWAVE simulates the combined effects of wave refraction-diffraction using the basic mild-slope equation, the model formulation has been extended to include effects of wave dissipation by friction and breaking, and nonlinear amplitude dispersion. CGWAVE is a finite-element model and has been interfaced with the SMS (Surface water Modeling System) model (Jones & Richards, 1992) for pre-processing and post-processing. The classical super-element methods as well as a new parabolic approximation method developed recently (Xu, Panchang and Demirbilek 1995), are used in the treatment of the open boundary condition. An iterative procedure (conjugate gradient method) introduced by Panchang et al. (1991) and modifications suggested by Li (1994) are used in solving the discretized equations, which enables users to deal with simulations in very large spatial domains.

To better understand and solve the systemic problems (i.e. structural, erosion and scour, navigation problems in the inlet area) at Ponce de Leon Inlet, Florida, the Army Corps of Engineers constructed a physical model at the U.S Army Engineer Waterways Experiment Station (WES) facilities. Several computations and other studies were

conducted on this physical model with different numerical models (Smith and Harkins, 1997) and the results were compared to actual wave heights recorded at wave gauges in different locations of the physical model. But these numerical studies used coarse grid models, poorly simulated to represent the complex bathymetry. Also, laboratory experiments are not necessarily less expensive than field measurements, but provide a controlled environment for expeditiously testing a large number of different wave conditions and data for evaluating numerical models. This provided an excellent opportunity to apply the numerical wave prediction model CGWAVE to a real world application such as Ponce de Leon Inlet.

In the laboratory study of Ponce de Leon Inlet, (also called the physical model), a 1:100 scaling was used (Figure 1). Wave heights were measured offshore near the north jetty, and along the bounding shorelines. The study considered both monochromatic and spectral wave conditions of a wide range of wave periods and directions. In the present study, numerical predictions of CGWAVE model were extracted along Transects 1 and 2 where a number of measured gauge data were available from the physical model study. See Figure 1 for the locations of Transects 1 and 2 at Ponce de Leon Inlet.

The main objectives of this research were to:

- a) validate CGWAVE model in a real world application in the Ponce de Leon Inlet, Florida, where measured wave data existed.
- b) assess CGWAVE model's ability for simulating irregular sea states (spectral waves) at Ponce de Leon Inlet.

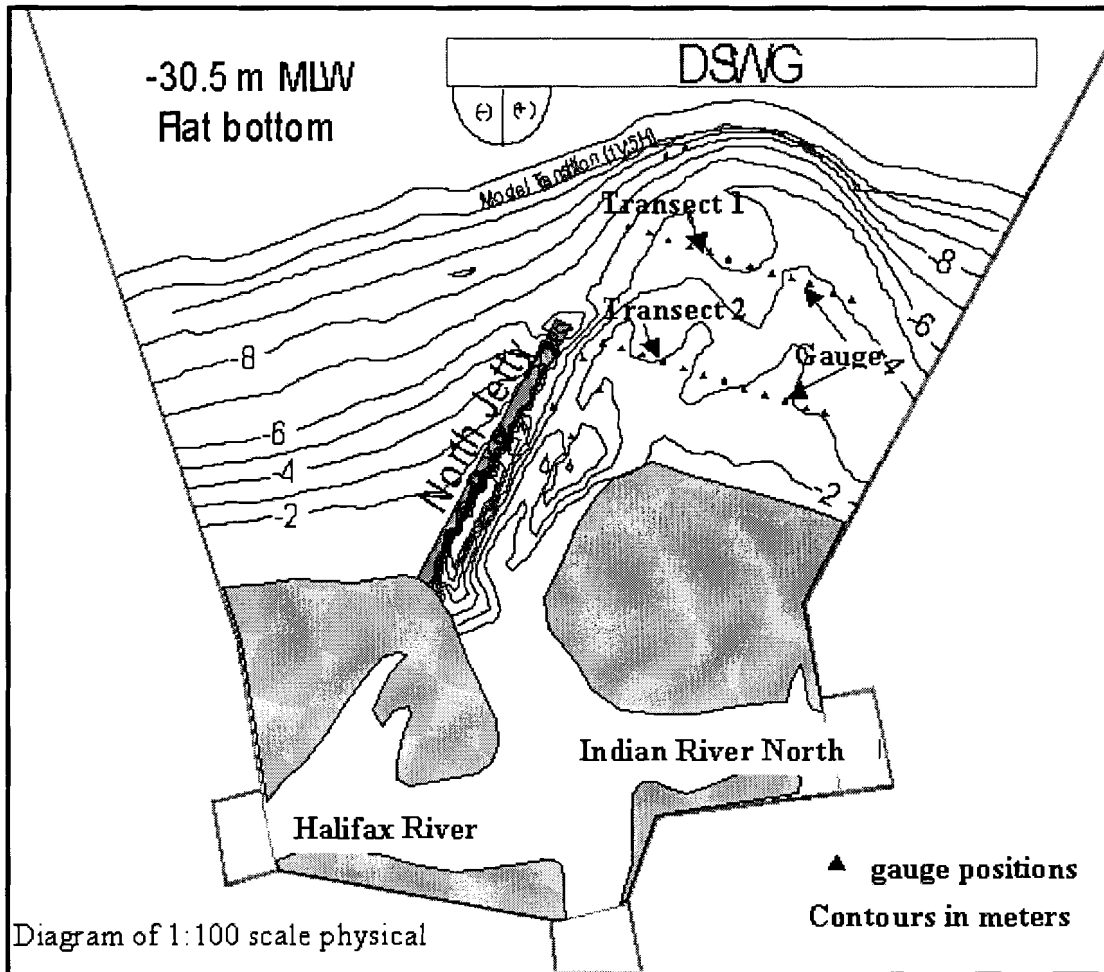


Figure 1. Physical model of Ponce Inlet (Reference)

c) investigate differences in the numerical model predictions for monochromatic and spectral waves at Ponce de Leon Inlet.

d) evaluate model estimates with wave breaking formulas at Ponce de Leon Inlet.

The layout of this thesis is as follows. A review of the Ponce de Leon Inlet physical model study is given in Chapter 2. A brief summary of CGWAVE model features is provided in Chapter 3. Grid generation for Ponce de Leon Inlet and other modeling details are discussed in Chapter 4. Results, including a comparison between numerical model and measured data, are discussed in Chapter 5. Concluding remarks and discussions are presented in Chapter 6.

Chapter 2

PHYSICAL MODEL PONCE DE LEON INLET

2.1. Summary of Physical Model Study

The Army Corps of Engineers constructed a 1:100 scale physical model of Ponce de Leon Inlet at the U.S Army Engineer Waterways Experiment Station (WES) facilities. The physical model domain was approximately 5.0 km along-shore and approximately 2.5 km cross-shore (prototype). Depth contours in the physical model study ranged from 30.5 m offshore to 0.0 m at the shoreline. Bathymetric contours in the physical model begin from positive elevations to -10.7 m Mean Low Water (MLW), from where a planar slope of 1V: 5H transitions it to a flat basin bottom with prototype elevation -30.5 m MLW (also denoted as 30.5 m depth in this thesis). A correction of 1m to these “base” depths to accommodate tidal influences was also done. The model bathymetry was derived from a 1994 airborne laser (lidar) survey data, and was constructed by molding a concrete veneer to conform to cross-shore cross-sections having a 1.2-m (model-scale) long shore spacing. An impermeable vertical structure with small (1cm) stones sloped on either side was used to represent the north jetty. Figure 1 shows the study layout and main features represented in this 1:100 scale physical model study. A directional spectral wave generator (DSWG) was used to generate waves in the physical model. Additional details of the physical model set up, characteristics of the model basin, wave generator, gauges and other instrumentation used in this study have been described elsewhere (Smith and Harkins, 1997).

Various factors can create differences between the prototype, the physical model and the numerical model. The potential effects of model scaling and other modeling effects have not been addressed in the comparison of the measured data to numerical predictions described in this thesis. For instance, in the laboratory study, diffraction may have occurred at the ends of the wave generator because of its finite length. In the real world and in the numerical model, there is no such finite length limitation while describing incident waves. To avoid these diffractive effects, incident wave directions were limited to ± 30 degrees from a line perpendicular to the wave generator. Attempts were made to place wave energy-absorbing mats along the lateral boundaries of the basin to minimize reflections from the model study boundaries, but the effectiveness of absorbers were not addressed in the U.S Army Engineer Waterways Experiment Station (WES) (Personal communication with Demirbilek).

2.2. Characteristics of Measured Data

Waves were generated seaward of the planar transition by a 27.4 meter long Directional Spectral Wave Generator (DSWG) placed in 30.5 m water depth. The DSWG is an electronically controlled, electro-mechanical system capable of producing directionally spectral waves by a time series of paddle displacement transmitted to each of 60 paddles. The orchestrated wave paddle movements produce the specified incident two-dimensional wave spectra, $S(f,\theta)$. Here f is the wave frequency, and θ is the wave direction. The TMA shallow-water frequency distribution (Bouws et al. 1985) and the wrapped normal directional spreading function (Borgman 1990) were used in the generation of directional spectrum $S(f,\theta)$.

Different empirical formulas are available to describe wave frequency spectra in deep water, in intermediate water depths, and in shallow water depths. The TMA spectral shape is considered to be appropriate for shallow depths such as for Ponce de Leon Inlet (Brows et al 1985). As regards the directional spreading, this may be assumed of the form of a cosine² distribution or a wrapped normal distribution. Three 2d spectral simulations were performed for each spectral case, by combining the TMA frequency spectra and the wrapped normal directional distribution as described below.

$$S(f, \theta) = E(f) \times D(\theta) \quad (1)$$

where

$S(f, \theta)$ (m²/Hz/rad.) = spectral energy for a wave component with frequency f

and direction θ

$E(f)$ (m²/Hz) = spectral density

f (Hz) = frequency

$D(\theta)$ (1/rad.) = angular spreading functions

θ (deg.) = the angle made with the mean direction

$$E(f) = \alpha g^2 (2\pi)^{-4} f^{-5} \exp \left\{ -1.25 \left(\frac{f_m}{f} \right)^4 + (\ln \gamma) \exp \left[\frac{-(f - f_m)^2}{2\sigma^2 f_m^2} \right] \right\} \delta(f, h) \quad (2)$$

α (dimensionless) = phillips constant

σ (dimensionless) = shape parameter ($\sigma = \sigma_a$ if $f < f_m$ and $\sigma = \sigma_b$ if $f \geq f_m$)

γ (dimensionless) = peak enhancement factor

$\delta(f, h)$ (dimensionless) = is a factor that incorporates the effect of depth h and may be approximated as:

$$\delta = 0.5(\omega_h)^2 \text{ for } \omega_h < 1$$

$$\delta = 1 - 0.5(2 - \omega_h)^2 \text{ for } 1 \leq \omega_h \leq 2$$

$$\delta = 1 \text{ for } \omega_h > 2$$

where

$$\omega_h = 2\pi f (h/g)^{1/2} \text{ (dimensionless)}$$

h = is the effect of deep ocean depth (for Ponce de Leon Inlet $h = 31.5$ m)

The directional distribution (i.e. angular spreading) of spectral waves was based on the Wrapped Normal Distribution developed by Borgman (1991), which is defined as

$$D(\theta) = \frac{1}{2\pi} + \frac{1}{\pi} \sum_{j=1}^J \exp\left[-\frac{(j\sigma_m)^2}{2}\right] \cos j(\theta - \theta_m) \quad (3)$$

where

θ_m (deg.) = mean wave direction

J = number of terms in the series

σ_m = (deg.) spreading parameter

Overall, the match between the “target” theoretical spectrum and spectra that were actually generated in the physical model with the DSWG was reasonable as far as spectral shape is concerned. Although similar in shape, leakage beneath the paddles and mechanical losses in DSWG caused the magnitudes of the generated spectra to be less than those of the theoretical spectra. To compensate for these losses, gain factors were used by the Army Corps of Engineers, to correct the entire wave paddle time series signals produced by DSWG to the point until measured and theoretical spectra had

comparable magnitudes. Each TMA time series of wave conditions was approximately 17 minutes long, and this was equivalent to 2 hours 47 minutes in prototype scale.

At the Army Corps of Engineers, a set of 26 incident wave conditions was used in the physical model study to investigate the effects of wave height, wave period, wave direction, and directional spread; of these, 6 were considered for this study. The matrix of the incident wave conditions and associated parameters used in the physical model study is presented in Table 1 (Smith and Harkins, 1997). Cases 1, 2 and 3 in Table 1 are incident wave conditions and associated parameters for monochromatic simulations. Cases 4, 5 and 6 in Table 1 are incident wave conditions and associated parameters for spectral simulations. These 6 cases were simulated using the numerical model CGWAVE. The wave parameters listed in Table 1, H , T , θ , γ , σ_m , α , σ_a , σ_b , represent the incident significant wave height, wave period, wave direction, the Peak Enhancement Factor, circular deviation of the wrapped normal spreading function, Phillips constant, and shape parameter respectively; these parameters are used to calculate $S(f, \theta)$. The resulting wave height

$$H_s = 2 \int S(f, \theta) df d\theta \quad (4)$$

The Army Corps of Engineers ran twice to ensure the repeatability of signal generation by DSWG. Please note that the Ponce de Leon Inlet domain angle orientation for the wave direction parameter θ in CGWAVE is shown in Figure 2.

Table 1. Monochromatic and Spectral Input Wave Conditions (Reference)
Prototype Scale

Case #	H (m)	T (sec)	θ (deg)	γ	σ_m (deg)	α	σ_a	σ_b
1	0.95	8	270	Mono	1	N/A	N/A	N/A
2	0.93	10	270	Mono	1	N/A	N/A	N/A
3	0.78	15	270	Mono	1	N/A	N/A	N/A
4	1.01	8	240	3.3	30	0.000899	0.07	0.09
5	0.95	10	270	5.0	20	0.000383	0.07	0.09
6	0.76	15	300	7.0	10	0.000124	0.07	0.09

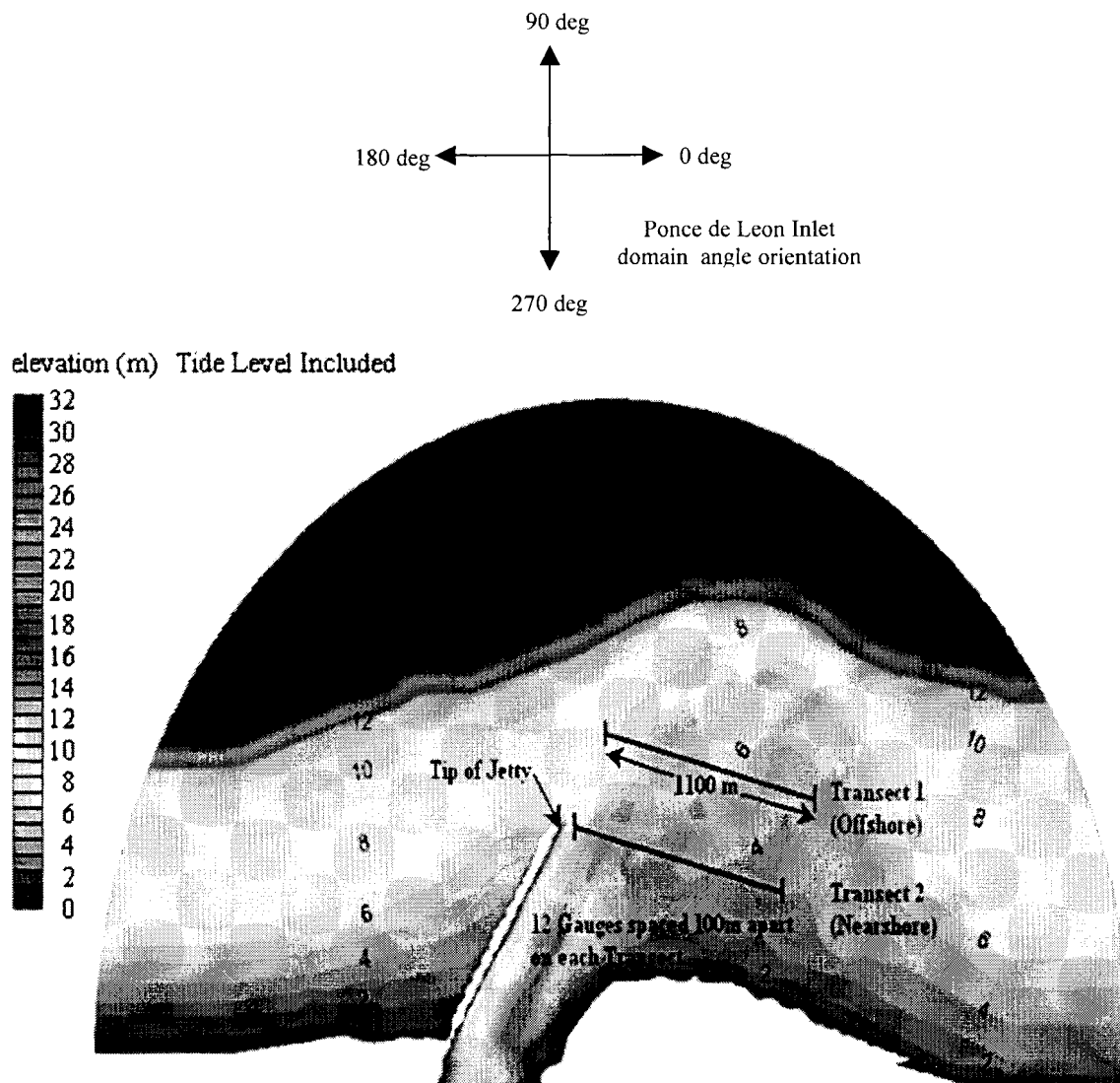


Figure 2. Contours and orientation of numerical model Ponce de Leon Inlet

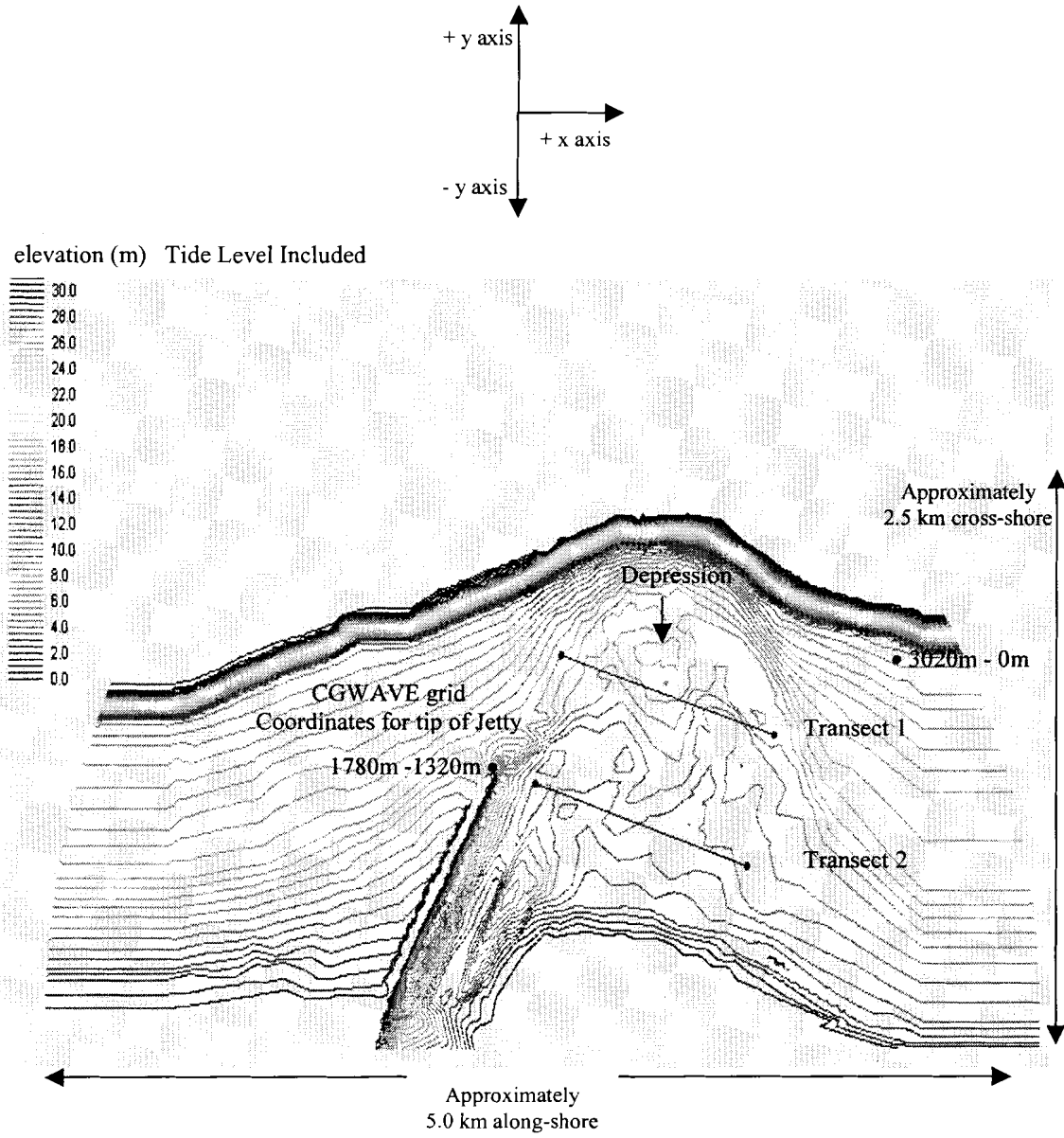


Figure 3. Contours and features of numerical model Ponce de Leon Inlet

Wave data were collected using 30 capacitance wave gages and a sampling frequency of 25 Hz. Twenty-four gages were placed along two linear arrays, denoted in this thesis as Transects 1 and 2 (see Figure 1), and the gauge spacing was 100-meter in prototype scale. Of the remaining gages, two were placed immediately shoreward of the model transition (for verification of input conditions) and four were placed in the lee of the jetty inside the throat area (not studied in this thesis). Water surface displacement at each gauge was analyzed in the time and frequency domains. In the time domain, a down-crossing analysis was performed and H_s was calculated for monochromatic wave cases. For the spectral wave cases (case 4, 5 and 6 in Table 1), wave spectra were calculated using a Fast Fourier Transform technique, FFT. Details of data analysis may be found elsewhere (Smith and Harkins, 1997).

Chapter 3

THE NUMERICAL MODEL CGWAVE

3.1. Background

Reliable estimation of the wave conditions in and around harbors is vital to the success of harbor operations. For reasons that were stated in Chapters 1 and 2, this estimation must often be accomplished using mathematical modeling techniques. However, most harbors confront the modeler with numerous complexities (Panchang & Demirbilek, 2001). Geometrically, as may be seen in Figures 1, 2 and 3, the domain of a harbor in numerical modeling may include arbitrary coastlines and bathymetric features, and man-made structures such as piers, jetties, breakwaters, etc. These features may induce wave refraction, diffraction, reflection, and dissipation by friction and breaking, to varying degrees. The incident waves of interest may cover a wide spectrum of frequencies, from very short waves to extremely long period waves that could cause harbor resonance, and incident waves may approach a harbor from any direction. For simulating short waves, the number of grids required for properly resolving waves can be extremely large, making the modeling a challenging task. Longer period waves may need fewer grids, but these require a more realistic specification of the boundaries to account for reflections that may occur from structures, coastlines, and bathymetric slopes. In addition to these complexities, modelers may have to account for the effects of interaction between wave frequencies and wave-current interaction that could affect waves in the domain.

3.2. Model Description

The model CGWAVE was developed at the University of Maine under a contract for the U.S. Army Corps of Engineers, Waterways Experiment Station (Demirbilek and Panchang, 1998). It is a general purpose, state-of-the-art wave prediction model applicable to the estimation of wave fields in harbors, open coastal regions, coastal inlets, around islands, and around fixed or floating structures (Panchang, Xu and Demirbilek, 1999; Panchang and Demirbilek, 2001). While CGWAVE simulates the combined effects of wave refraction-diffraction included in the basic mild-slope equation, it also considers effects of wave dissipation resulting from friction and breaking, nonlinear amplitude dispersion, and harbor entrance losses. CGWAVE has finite elements and is interfaced with Surface Water Modeling System (SMS) (Jones & Richards, 1992) for graphics and efficient implementation of pre-processing and post-processing tasks. This enables modelers to efficiently simulate waves in very large spatial domains. The following sections provide a brief review of the basic theory for the numerical model CGWAVE.

3.3. Fundamental Equations

The solution of the two-dimensional elliptic mild-slope wave equation (MSE) is a well-accepted method for modeling surface gravity waves in coastal areas (e.g. Chen & Houston, 1987; Chen, 1990; Xu & Panchang, 1993; Mei, 1983; Berkhoff, 1976; Kostense et al., 1986; Tsay and Liu, 1983; Demirbilek and Panchang, 1998; Panchang and Demirbilek, 1999 and 2001).

In its basic form, the methodology is based on solving the following two-dimensional elliptic mild-slope wave equation:

$$\nabla \cdot (CC_g \nabla \phi) + k^2 CC_g \phi = 0 \quad (5)$$

where

$$\phi(x,y) \text{ (m}^2/\text{s)} = \text{complex surface elevation function } (= \phi_1 + i\phi_2)$$

$$i = \sqrt{-1}$$

$$\sigma \text{ (1/s)} = \text{wave frequency under consideration}$$

$$C(x,y) \text{ (m/s)} = \text{phase velocity} = \sigma/k$$

$$C_g(x,y) \text{ (m/s)} = \text{group velocity} = \partial\sigma/\partial k$$

$$L \text{ (m)} = \text{wavelength}$$

$$k(x,y) \text{ (1/m)} = \text{wavenumber } (=2\pi/L), \text{ related to the local depth } d(x,y) \text{ through the dispersion relation:}$$

$$\sigma^2 = gk \tanh(kd) \quad (6)$$

$$g \text{ (m/s}^2\text{)} = \text{gravitational constant}$$

The wave height H (m) can be obtained from the complex surface elevation function ϕ as follows:

$$H = \frac{2\sigma}{g} \sqrt{(\phi_1^2 + \phi_2^2)} \quad (7)$$

Essentially (5) represents integration over the water column of the three-dimensional Laplace equation used in potential wave theory. The integration, originally described by Berkhoff (1976) and Smith and Sprinks (1975), is necessary

because the solution of the three-dimensional problem is computationally difficult for harbors with a characteristic length that is several times the wavelength. The integration is based on the assumption that the vertical variation of the wave potential is largely the same as that for a horizontal bottom, i.e.

$$\phi(x, y, z) \approx \frac{\cosh k(d+z)}{\cosh kd} \phi(x, y) \quad (8)$$

This approximation is obviously valid for a "mild slope", characterized by $|\nabla d|/kd \ll 1$, a criterion that is usually met in most practical applications. Being elliptic, (5) represents a boundary value problem, which can accommodate internal nonhomogeneities. It hence forms a widely used basis for performing wave simulations in regions with arbitrarily shaped (manmade or natural) land boundaries and arbitrary depth variations. Unlike "approximate" mild slope wave models, better known as the parabolic models (e.g. REFDIF and RCPWAVE used by Smith and Harkins, 1997) there are no intrinsic limitations in (5) concerning the shape of the domain, incident wave angle, or the degree and direction of wave reflection and wave scattering. While it is valid for a monochromatic wave condition (single incident frequency-direction), irregular wave conditions can also be simulated using (5) by the superposition of monochromatic wave simulations.

For including nonlinear mechanisms in the MSE, Panchang and Demirbilek (2001) considered the following extended form of (5):

$$\nabla \cdot (CC_g \nabla \phi) + (k^2 CC_g + iC_g \sigma W) \phi = 0 \quad (9)$$

in which a dissipation term W (1/m) has been included. It may represent breaking and/or friction and is described later in section 3.6.

Several computational models based on (5) or (9) have been developed in recent years (e.g. HARBD, PHAROS, REFDIF, RCPWAVE etc.). These models differ in the choice of the numerical methods (e.g. finite-difference method, boundary element method, finite element method), boundary conditions, in the manner the linear system of equations are solved, and how additional mechanisms are considered. While a detailed comparison of these models is outside the scope of this thesis, a brief summary of various features pertaining to CGWAVE is discussed next. For a detailed review and comparison of these models, see Panchang and Demirbilek (2001).

3.4. Treatment of Boundary Conditions

CGWAVE uses a triangular finite-element formulation with grid sizes varying throughout the domain based on the local wavelength. The model allows one to specify the desired reflection properties along the coastline and other internal boundaries via a Robbins' type boundary condition ($\delta \phi / \delta n = \alpha \phi$, where α is related to the reflection coefficient). Domains on which the elliptic equation (5) and (9) is solved are enclosed in a semi-circle by boundaries such as coastlines and surface-penetrating structures (jetties, breakwaters, seawalls, etc.) and open boundaries representing artificial boundaries that separate the modeling area from the sea region outside (Figure 4). A creek or tributary at

the back bay or down wave end of the domain may be considered as a fully absorbing boundary. An open ocean boundary is where incident wave is specified and waves may radiate out through such boundary. Along all open and land boundaries, appropriate conditions must be specified to solve (5) and (9); however, only approximate boundary conditions can be developed for them. The input conditions are provided at the offshore ends of two one-dimensional cross-shore sections shown as Transects 1 and 2 in Figure 4. (In practice, the input condition is known at the end of one of the transects. The condition at the offshore end of the other transect is obtained by appropriate phase translation.) A combination of the incident and reflected waves is computed along these transects using a one-dimensional version of (5) and (9); this partial solution is then mapped on to the semicircle to force the two-dimensional model. The remainder of the solution on the boundary consists of a scattered wave that emanates from within the domain; this component is allowed to radiate out through the use of an impedance boundary condition. (For detailed descriptions, see Panchang et al. 2000; Zhao et al. 2001; and Panchang and Demirbilek, 2001).

3.4.1. Land (Closed) Boundary Conditions

Along a coastline or surface-protruding structure, the following boundary condition has been traditionally used (e.g. Berkhoff 1976; Tsay & Liu 1983; Tsay et al. 1989; Oliveira and Anastasiou 1998; Li 1994a)

$$\frac{\partial \phi}{\partial n} = \alpha \phi \quad (10)$$

where n is the outward normal to the boundary and α is related to a user-specified reflection coefficient defined as

$$\alpha = ik \frac{1-K_r}{1+K_r} \quad (11)$$

In (11), K_r varies between 0 and 1 and specific values for different type reflecting boundaries have been compiled by Thompson et al. (1996). In this research, the reflection coefficient was assumed to not depend on incident wave angle. Chen (2002) has recently developed a new type reflection boundary condition depending on the local wave angle. For details about the treatment of boundary conditions, please refer to Panchang & Demirbilek (2001).

3.4.2 Open Boundary Conditions

Along an open boundary of the model (see Figure 4), the incident wave ϕ_i must be specified. Typical harbor applications generally use model domains such as that described in Figure 4, where the semicircle boundary is used to separate the model area from the open sea. In the exterior domain Ω' the potential ϕ is comprised of three components (Demirbilek and Panchang, 1998):

$$\phi = \phi_i + \phi_r + \phi_s \quad (12)$$

where

ϕ_i = the incident wave that must be specified to force the model,

ϕ_r = a reflected wave that would exist in the absence of the harbor, and

ϕ_s = a scattered wave that emanates as a consequence of the harbor and must satisfy

3.5. Numerical Solution Scheme

Equation (8) is generally solved using either the finite-difference method or the finite element method. In general, finite-difference discretizations are not well suited to represent the complex domain shapes described in Figure 1, 2 and 3. Not only are the boundaries distorted, but the number of uniformly spaced grids may also be excessively large. Adequate resolution, typically 10 points per wavelength, demands that the spacing be determined from the smallest wavelength. Finite element models, on the other hand, allow the construction of grids with variable sizes (based on the local wavelength) and give a good reproduction of the boundary shapes. Like most finite element models (e.g. Tsay and Liu 1983; Tsay et al. 1989; Kostense et al. 1988), CGWAVE uses triangular elements, and the model has been interfaced with modern graphical grid generating software that permits efficient and accurate representation of harbors with complex shapes. This software, called the Surface-water Modeling System, SMS (Zundel et al., 1998; and Jones and Richards (1992) that can be used to conveniently generate as many as a million elements of varying size, based on a desired grid resolution specified by the user.

The numerical treatment of (5) with appropriately chosen boundary conditions leads to a system of linear equations in the general form as:

$$[A] [\phi] = [B] \quad (13)$$

where $[\phi]$ represents the vector of all the unknown potentials, i.e. wave height in our case. For solving (9), a similar system results as long as W is prespecified. The

matrix $[A]$ is usually extremely large and therefore in earlier models (e.g. Tsay and Liu 1983; Tsay et al. 1989; Chen, 1990; Chen and Houston, 1987), the solution of (13) could only be obtained by Gaussian Elimination method, which requires enormous memory and is not possible when the number of wavelengths in the domain is large (i.e. short waves or a large domain).

In CGWAVE, the solution of (13) has been obtained with a minimal storage requirement for the matrix $[A]$. This is due to the development by Panchang et al. (1991) and Li (1994a) of iterative techniques especially suited for problems such as (5). These techniques, based on the conjugate gradient method, guarantee convergence and, according to the review of Panchang & Demirbilek (2001), it is extremely robust in a wide variety of applications involving both finite differences and finite elements for several kinds of boundary conditions.

For modeling spectral wave conditions, the input spectrum can be discretized into several components, and each component may be modeled as a monochromatic wave by methods described above. The total solution by the model for a spectral sea state, known as significant wave height, at any grid point may be calculated by linear superposition of the spectral component solutions as described later in Chapter 4.

In this research, a super-computer spectral version of CGWAVE model was used in which significant improvements in computational speed were obtained by using two-level code parallelization for operation on high performance parallel computing platforms

such as the SGI/Cray Origin2000 (O2K). Details regarding the parallelization may be found in Bova et al. (2000), who reported a reduction in run times by a factor of 250-580 compared with serial codes. For the application at Ponce de Leon Inlet (Florida), which has a maximum of nearly 300 input spectral components, CGWAVE was solved on an approximately 5.0 km along-shore (x-axis) and approximately 2.5 km cross-shore (y-axis) domain (Figure 3) containing 265,000 nodes in 72 hours. With the recently developed super-fast solvers, the run time for this problem has been lowered to 3 hours. This fast version was available for the present study on the DOD supercomputer at the Army R & D center.

3.6. Wave Breaking Schemes

Several investigators (e.g. de Girolamo et al. 1988; Massel 1992; Isobe 1999; and Chawla et al. 1998) have proposed that breaking can be introduced in the mild-slope equation (5). They used a parameterized dissipation term as follows:

$$\nabla \cdot (CC_g \nabla \phi) + (CC_g k^2 + iC_g \sigma \gamma) \phi = 0 \quad (14)$$

γ (1/m) = wave breaking factor = W (1/m) if no friction is present

The wave breaking factor γ contained in the last term of (14) can be parameterized in several ways. However, all parameterizations are a function of the wave height and so combined the model becomes nonlinear.

Zhao et al. (2001) developed a technique for including the effects of dissipation due to wave breaking in CGWAVE. Zhao et al. (2001) developed ways to handle the

nonlinearity and examined five breaking parameterizations of waves; two wave-breaking criteria are examined in this study because Zhao et al. found them to be most robust. These are the criteria of Battjes and Janssen (1978), denoted (BJ), and by Dally et al. (1985), denoted (DDD). However, their results can be somewhat different, and hence their effects on Ponce results are examined. Numerical model results described in Chapter 5 were obtained using both wave-breaking formulas for monochromatic cases and only DDD breaking was used for spectral cases.

Chapter 4

GRID GENERATION FOR CGWAVE USING SURFACE-WATER

MODELING SYSTEM (SMS)

A detailed description of the two-dimensional grid used in CGWAVE model for Ponce de Leon Inlet is presented here. The model CGWAVE has been interfaced with the grid-generation and visualization package called SMS (Surface Water Modeling System), a general-purpose graphical user-interface for flow modeling (Jones & Richards, 1992).

4.1. Overview of SMS

SMS contains numerous two-dimensional (2D) hydrodynamic models and supports these as a general-purpose grid generation and visualization package. It includes capabilities for generating grids for finite element and finite difference flow (hydrodynamic) and wave models. Several utilities in the form of Fortran programs were developed for interfacing CGWAVE model to SMS. For example, given a bathymetric data set (XYZ coordinate file), these programs can generate a wavelength-dependent triangular finite element mesh for a user-specified resolution, i.e. number of points per wavelength. The capability for constructing a semi-circular open boundary, assigning reflection coefficients along coastal boundaries, and eliminating unwanted land points from the meshing area, exists in SMS and grids for an application can be generated in a few hours. The finite element grid and boundary specification data from SMS constitute the main input of CGWAVE. At present, the SMS interface does not support the

generation of spectral wave input for CGWAVE model, and this can be done using one of the Fortran programs developed in this study. The output of CGWAVE can be processed in SMS. Different Graphical User Interface (GUI) capabilities available in SMS make the implementation of the model very efficient, and allow users to quickly view and analyze the model solution.

4.2. Numerical Model Grid Generation Using SMS

For Ponce de Leon Inlet, the modeling domain covered a region of the inlet that extended approximately 5.0 km along-shore and approximately 2.5 km cross-shore (Figure 3). The bathymetry data were obtained from the Army Corps of Engineers in the form of XYZ coordinates, where x- and y-coordinates are the horizontal coordinates, and z is the depth, and all are in units of meters. For computational purposes, a cut off depth of 0.275 m was used for the land-water interface. Depths below 0.275 m (i.e. from 0 m to 0.275 m) were assumed to contribute little to numerical results for the periods of interest; since resolving them also increases unnecessary computational time, they were eliminated.

The water depth at the land boundaries was 0.275 m and the deepest depth offshore was about 31.5 m. A tide elevation of 1.07 m was added to water depth values to account for the effects of tidal variations as was done in the laboratory study. The resolution of the finite element grid was made to be dependent on local water depth and incident wave period. As a rule of thumb, CGWAVE requires approximately 10 points

per wavelength for its grids, and in the areas of strongly varying bathymetry, or in shallower depths the higher the grid resolution the better the model results.

Since grid resolution has a paramount effect on the accuracy and reliability of model results, we examined the influence of grid resolution on CGWAVE predictions by testing three grids, Grid 1, 2 and 3 with different resolutions. Grid #1 had 118,266 nodes and 234,696 triangular elements, Grid #2 had 227,138 nodes and 452,436 triangular elements, and Grid #3 had 265,119 nodes and 528,398 triangular elements. Information about grids is summarized in Tables 2-4. These tables provide the percentages of areas in the grids that satisfy a certain resolution (i.e. points per wave length). Ideally, the grids should have no less than 10 points per wavelength to ensure accuracy of modeling predictions. As we can see from Tables 2-4, parts of each grid did not fulfill this requirement, and model predictions in those areas with less resolution may be unreliable. In principle, it should be possible to generate a modeling grid that has 10 points per wavelength everywhere in the domain. However, such a high-resolution grid may not be useful if it exceeds available computational resources (i.e. it takes too long to compute the solution for a large number of triangular elements in the computational domain). Thus, a compromise is necessary in practice between the grid resolution required and the computational resources available. Sensitivity tests (not shown in this thesis) indicated that Grids #1 and 2 were inadequate, and therefore Grid #3 with the best resolution has been used in the comparison of model and data. It can be seen from Tables 2, 3 and 4 that Grid #3 has the best overall resolution since it provides the highest percentage distribution of points per wavelength to meet the 10-points per wavelength requirement.

Therefore, Grid#3 was selected for the prediction of wave heights and directions in both monochromatic and spectral simulation (Table 1).

4.3. Creating Spectral Components

Storms or sea states representing real waves in nature may be simulated with CGWAVE. This requires a proper specification of the corresponding sea state spectra and the discretization of spectra into components in frequency and angular direction (i.e. spreading) space. Such a decomposition of the wave spectra is frequently used to characterize real ocean waves generated by the winds. For example, for 10 frequency and 20 directional components, the total components would be $n_t = n_f \times n_a = 10 \times 20 = 200$, where n_f is the number of frequency components and n_a is the number of angular components. The actual number of components for all three spectral cases (Cases 4, 5 and 6 in Table 1) are presented later. The input wave amplitude (A) for a particular frequency component (f) with initial direction (θ) can be shown in equation (15) below:

$$A = [2E(f)D(\theta)\Delta f\Delta\theta]^{1/2} \quad (15)$$

Where

$E(f)$ and $D(\theta)$ are obtained with equations (2) and (3) in section 2.2.

Δf = frequency segment size

$\Delta\theta$ = directional segment size

Table 2. Resolution analysis for wave period 15 sec.

Points per wave length	Grid resolution for 15 second wave Percentage distribution of points per wave length distribution (%)		
	<i>GRID 1 (118266 nodes and 234696 elements)</i>	<i>GRID 2 (227138 nodes and 452436 elements)</i>	<i>GRID 3 (265119 nodes and 528398 elements)</i>
0 – 5	1.7	0.8	0.7
5 – 6	3.2	1.6	1.4
6 – 7	7.5	3.8	3.2
7 – 8	7.0	3.6	3.0
8 – 9	7.1	3.8	3.2
9 – 10	7.9	4.2	3.6
10 – 11	5.4	2.9	2.5
11 – 12	4.2	2.3	1.9
12 – 13	2.0	1.2	1.1
13 – 14	3.8	1.3	1.1
14 – 15	1.9	0.4	0.4
15 and up	49.8	74.1	77.9

Table 3. Resolution analysis for wave period 10 sec.

Points per wave length	Grid resolution for 10 second waves Percentage distribution of points per wave length distribution (%)		
	<i>GRID 1 (118266 nodes and 234696 elements)</i>	<i>GRID 2 (227138 nodes and 452436 elements)</i>	<i>GRID 3 (265119 nodes and 528398 elements)</i>
0 – 5	19.0	9.5	8.2
5 – 6	7.9	4.3	3.7
6 – 7	15.0	7.9	6.8
7 – 8	2.1	1.3	1.1
8 – 9	4.9	2.2	1.9
9 – 10	3.2	0.7	0.7
10 – 11	4.4	0.2	0.2
11 – 12	4.7	1.9	1.5
12 – 13	9.2	2.6	2.1
13 – 14	4.6	0.7	0.6
14 – 15	6.7	0.1	0.0
15 and up	18.2	68.6	73.5

Table 4. Resolution analysis for wave period 8 sec.

	Grid resolution for 8 second waves Percentage distribution of points per wave length distribution (%)		
Points per wave length	<i>GRID 1 (118266 nodes and 234696 elements)</i>	<i>GRID 2 (227138 nodes and 452436 elements)</i>	<i>GRID 3 (265119 nodes and 528398 elements)</i>
0 – 5	34.2	17.7	15.1
5 – 6	9.3	5.0	4.3
6 – 7	4.8	2.5	2.2
7 – 8	4.8	0.9	0.7
8 – 9	5.0	0.6	0.4
9 – 10	10.6	3.6	3.0
10 – 11	6.8	1.2	0.8
11 – 12	8.7	0.2	0.0
12 – 13	3.7	0.6	0.0
13 – 14	4.2	3.9	2.3
14 – 15	1.5	4.4	3.4
15 and up	6.6	59.6	67.8

The resulting wave heights at any location in the model domain are used to compute the significant wave heights (H_s) by summing up the heights of the individual frequency components as:

$$H_s = 2 \sum_1^n H_i \quad (16)$$

where

n = total number of frequency-direction components; and

H_i = the wave height corresponding to the i th component.

A two-dimensional spectra $S(f,\theta)$ of a sea state is constructed by multiplying $E(f)$ and $D(\theta)$. The CGWAVE input for such waves would consist of a set of discrete monochromatic wave components. These components may be simulated separately (since wave-wave interaction is not considered in CGWAVE), and results of these individual components may be combined as described above and the significant wave height computed in the modeling domain. The predicted wave direction for spectral simulations has been assumed to be the direction associated with the peak frequency of the incident waves. Therefore, the reported wave direction is an approximate value.

As mentioned earlier, three spectral cases were studied and the results are presented later on in this thesis. Creating the adequate number of spectral components using the TMA spectra equations mentioned in section 2.2 is a key element in spectral modeling. It is not computationally practical to create a spectra with very small Δf and $\Delta\theta$. Also, care should be taken not to create a spectra with insufficient number of frequency and directional components (i.e. large Δf and $\Delta\theta$ in the given and directional range). For example, consider case 4 in Table 1. The peak frequency for this case is 0.125 Hz or 8 sec and the mean wave direction for this case is 240 deg. We can create a spectral energy density $E(f)$ curve using the input parameters presented in Table 1 with a lower frequency range f_1 , an upper frequency range f_2 and a Δf using equation (2). Similarly we can create an angular spreading curve $D(\theta)$ using the input parameters in Table 1 with a lower directional range θ_1 , an upper directional range θ_2 and a $\Delta\theta$ using equation (3). If we select a lower and higher frequency around the peak frequency, $f_1=0.08$ Hz and $f_2=0.335$ Hz with a $\Delta f=0.015$ Hz. Therefore the total number of frequency bands is 18 ($(f_2 - f_1 / \Delta f + 1)$). Using equation (2) with the input parameters for case 4 shown in Table 1, we can create the following spectral energy curve as presented in Figure 5. Similarly, using equation (3) with the input parameters for case 4 shown in Table 1, we can create the following directional spectra curve as presented in Figure 6.

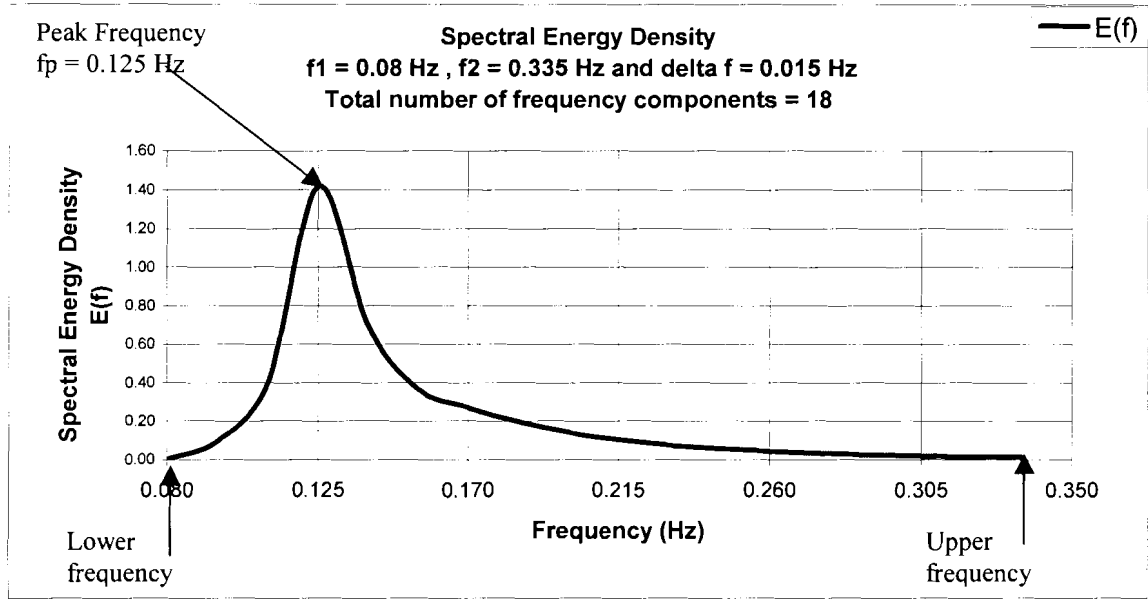


Figure 5. Spectral Energy Density for 18 frequency components

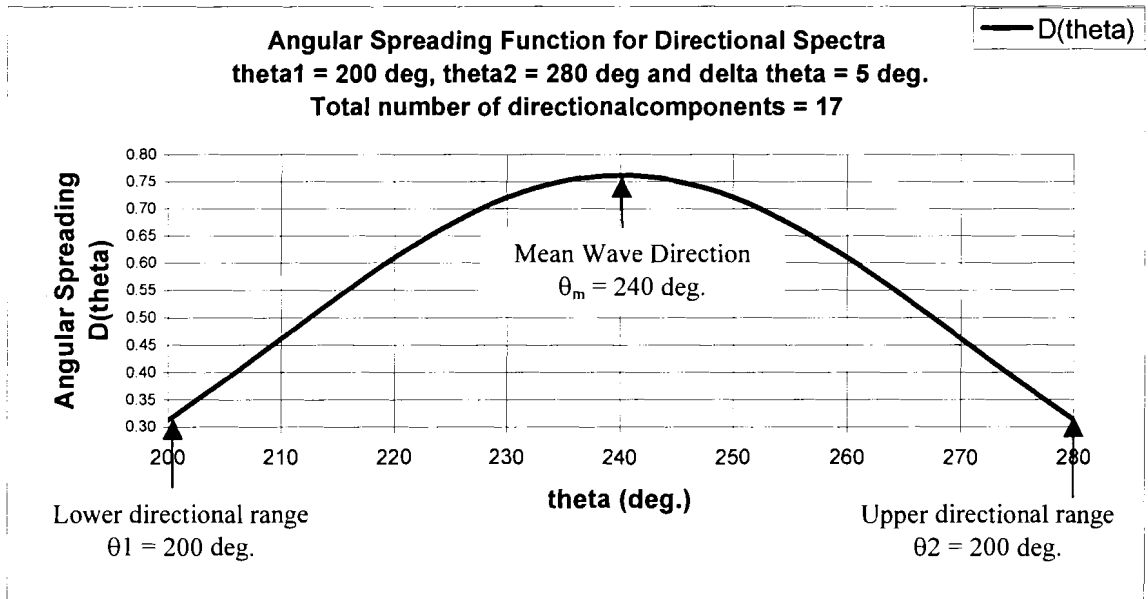


Figure 6. Directional Spectra for 17 directional bins

The directional spectra was created with $\theta_1 = 200$ deg. and $\theta_2 = 280$ deg. with a $d\theta = 5$ deg. Therefore the total number of directional bands = $17 (\theta_1 - \theta_2 / \Delta\theta + 1)$ and the total number of spectral components = total number of frequency bands x total number of directional bands = $18 \times 17 = 306$. The input wave amplitude (A) for each frequency component f (total of 18 frequency components f_1 to f_2) and direction component θ (total of 17 directional components θ_1 to θ_2) can be calculated using equation 21. Similarly, for all spectral case simulations, a spectrum was created and is presented in the results section.

Chapter 5

NUMERICAL PREDICTIONS

5.1. Monochromatic Wave Results

Wave heights for the entire Ponce de Leon Inlet domain can be computed, viewed and studied qualitatively. The SMS software package provides an excellent graphical interface for viewing and analyzing the results from CGWAVE. Figure 7 is a graphical representation of the estimated wave heights for the entire computational domain and Figure 8 is the wave phase diagram, which represents the pattern of the waves approaching the coastline for monochromatic case 1 (incident wave angle normal to the model at 270 degrees). The phase diagram (showing cosine of the phase) shows the expected bending of the phase lines due to refraction across the bathymetry, breaking around the jetty and also the expected decrease in the wavelength in the shoreward direction. The phase diagram also shows breaks near the transect (A in Figure 8), where bathymetry varies rapidly due to some shoals. Such phase diagram breaks, indicating crossing or multidirectional seas, have been observed in the labs (Berkhoff et al. 1982). Also, the phase diagram (not presented in this thesis) when the incident wave angle to the model domain is large (240 degrees and 300 degrees) shows greater refraction indicated by a bending pattern near the jetty as expected. Viewing and analyzing the results qualitatively for each monochromatic and spectral simulation enhanced the level of confidence that the wave height data obtained from the numerical model is reasonable. Amplitudes for spectral cases are smoother where bathymetry varies rapidly near the transects.

Since the qualitative examination for all CGWAVE numerical simulations presented reasonable results, only the figures for the monochromatic case 1 are presented in this thesis. The remaining part of the result section presents the actual numerical comparison between the wave height data from the numerical model and the actual gauges around Transects 1 and 2.

CGWAVE was used to predict the wave height for three monochromatic (single frequency spectra) real world wave simulations cases 1, 2 and 3 shown earlier in Table 1. The monochromatic results from the numerical model CGWAVE for all three cases are discussed in this section. Furthermore, for each monochromatic case, three simulations were computed, one in linear mode and two in the breaking mode. The two breaking models, Battjes and Janssen (1978) referred to as BJ and Dally et al. (1985) referred to as DDD, were discussed earlier in sections 3.6.

The input and boundary conditions used for the three monochromatic simulations are summarized in Table 5. A reflection coefficient of 0.95 was used for the jetty (i.e. nearly fully reflective structure), and 0 (fully absorbing) for the coastlines (Table 5). A rather high value for the reflection coefficient was used for the jetty because high reflections were observed in the laboratory tests. Similarly, a fully absorbing boundary condition was used for the coastal shorelines because of insignificant wave reflection observed during laboratory tests.

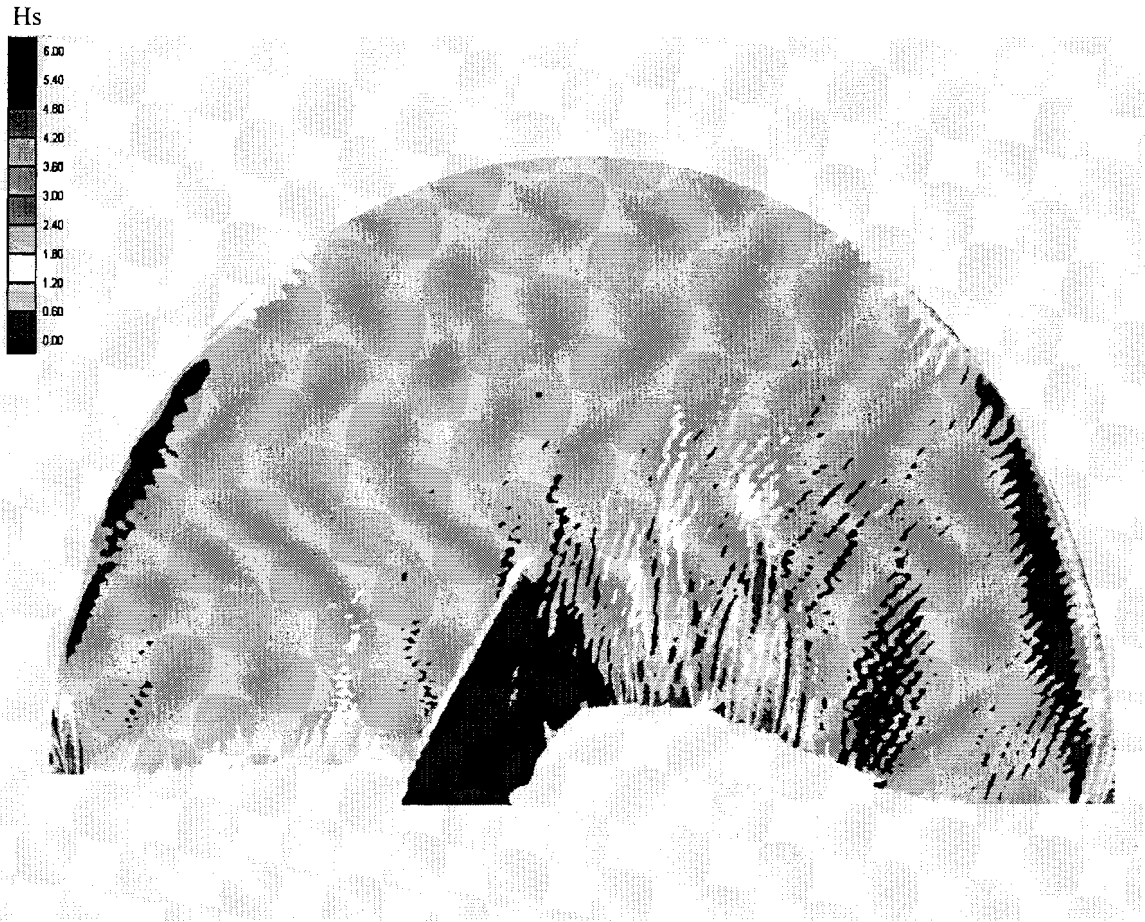


Figure 7. Estimated wave heights for Ponce de Leon Inlet from SMS

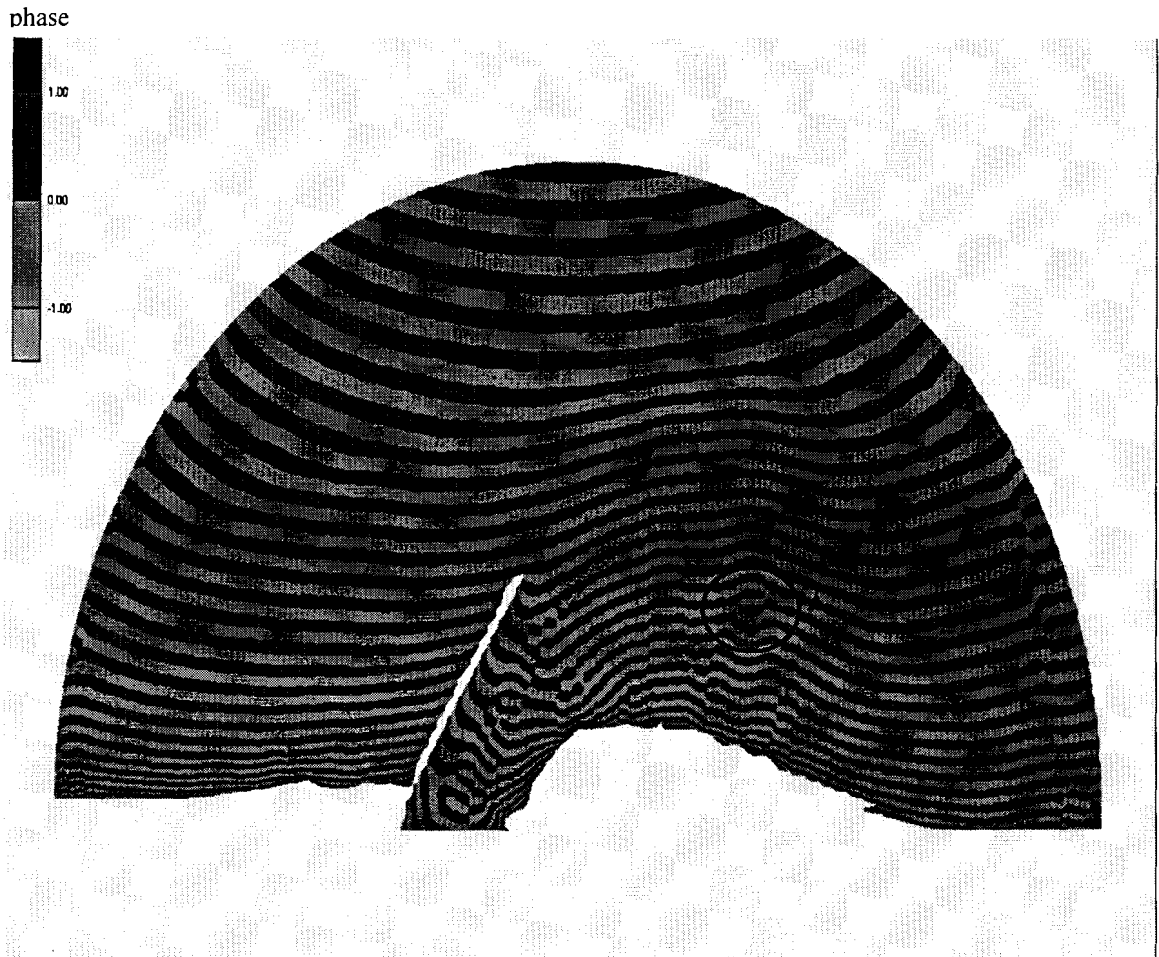


Figure 8. Estimated wave phase diagram for Ponce de Leon Inlet from SMS

Table 5. Summary of input and boundary conditions for monochromatic cases

Case Num.	Simulation Num.	CGWAVE Input Conditions				CGWAVE Boundary Conditions	
		Wave Period T_p (sec)	Incident Wave Direction θ_m (deg)	Wave Height H_m (m)	Type (linear/ breaking)	Coastline Reflection Coefficient	Jetty Reflection Coefficient
1. (Case 1 in Table 1)	1	8	270	0.95	linear	0.0	0.95
	2	8	270	0.95	breaking (DDD)	0.0	0.95
	3	8	270	0.95	breaking (BJ)	0.0	0.95
2. (Case 2 in Table 1)	1	10	270	0.93	linear	0.0	0.95
	2	10	270	0.93	breaking (DDD)	0.0	0.95
	3	10	270	0.93	breaking (BJ)	0.0	0.95
3. (Case 6 in Table 1)	1	15	270	0.78	linear	0.0	0.95
	2	15	270	0.78	breaking (DDD)	0.0	0.95
	3	15	270	0.78	breaking (BJ)	0.0	0.95

Using CGWAVE's post-processing program, wave heights were extracted along Transects 1 and 2 (Figure 1 and 2). The wave heights extracted from the output of CGWAVE were compared graphically and statistically to the physical data recorded at various gauge locations on both transects. For graphical comparisons, physical model wave height measurements (collected at the Army Corps Engineers Waterways Experiment Station WES) are plotted along with CGWAVE's numerical model wave height results. For each case two sets of plots were created, Transect 1 and 2. Additionally, as mentioned above, for each transect plot, four sets of wave height data were plotted versus gauge distances. One set of linear wave height data, two sets of breaking data (DDD and BJ), and one set of physical model's wave height data.

For statistically quantifying the numerical model's performance, RMS wave height errors was used in the comparison presented with the physical data recorded at various gauge locations on both the transects. The numerical model prediction wave height value for each gauge location was taken as an average of 5 points closest to the gauge, with the middle point being centered around the gauge location along the transect. For example, for gauge location at 100 m, the 5 point wave height average from the CGWAVE model will be an average of wave heights at 96 m, 98 m, 100 m, 102 & 104 m.

The following plots and tables summarize results for the monochromatic cases (Table 5) mentioned above. For graphical results, CGWAVE model predictions have been compared against physical model data in Figures 9, 10 and 11 for Transect 1, and Figures 12, 13 and 14 for Transect 2. Statistical numerical model estimates (RMS wave

height errors) of the wave heights are presented in Table 6 for Transect 1 and Table 7 for Transect 2. Summary and discussions of the monochromatic results will be presented after the graphical figures and statistical tables for both transects.

In general, the numerical predictions agree reasonably well with the physical model data, especially in the cases for Transect 1. Strong gauge-to-gauge variability is evident at Transect 2 in monochromatic simulations (Figures 12, 13 & 14), and these could be attributed to several factors. First, the bathymetry at Ponce Inlet is rather complex, especially around Transect 2. Second, the tip of the north jetty extends into the modeling domain to near the start of Transect 2 (Figure 3). The jetty further adds to the complexity of bathymetry and resulting wave field along Transect 2. Third, reflection coefficients and the degree of permeability offered by the jetties or breakwaters are not well understood in the studies of wave-structure interaction. In spite of these uncertainties, model results are fairly representative of the data. Results with breaking (BJ and DDD) show a considerable improvement at Transect 2 for wave periods $T_p=10$ and 15 sec.

In contrast, wave breaking does not appear to improve model-data comparison for the shorter wave period simulation with $T_p=8$ sec. This is evident since little or no breaking has occurred along Transect 1, and results with and without breaking appear to be indistinguishable. It should be noted that the exterior sea is bounded in the physical model, preventing the radiation of waves out to the open sea.

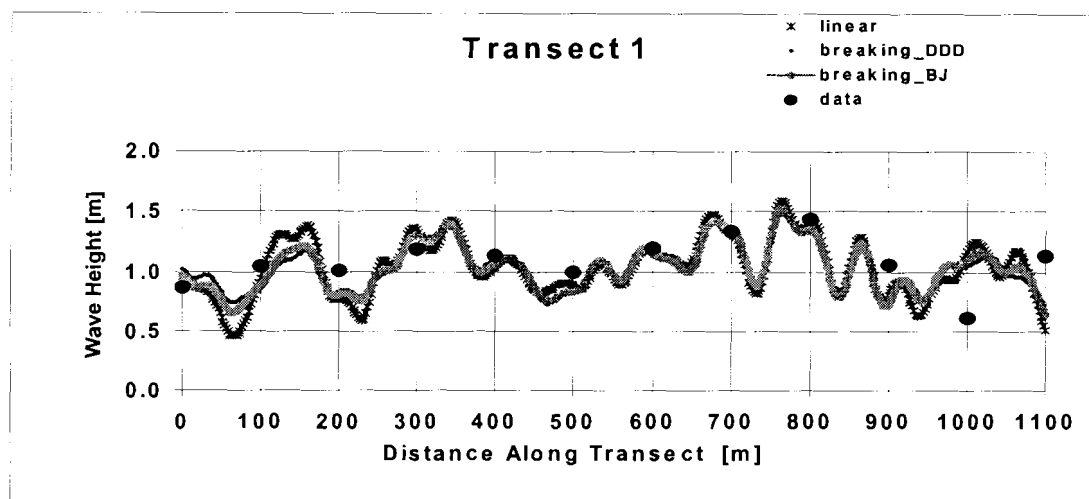


Figure 9. Wave height for Transect 1 monochromatic case 1

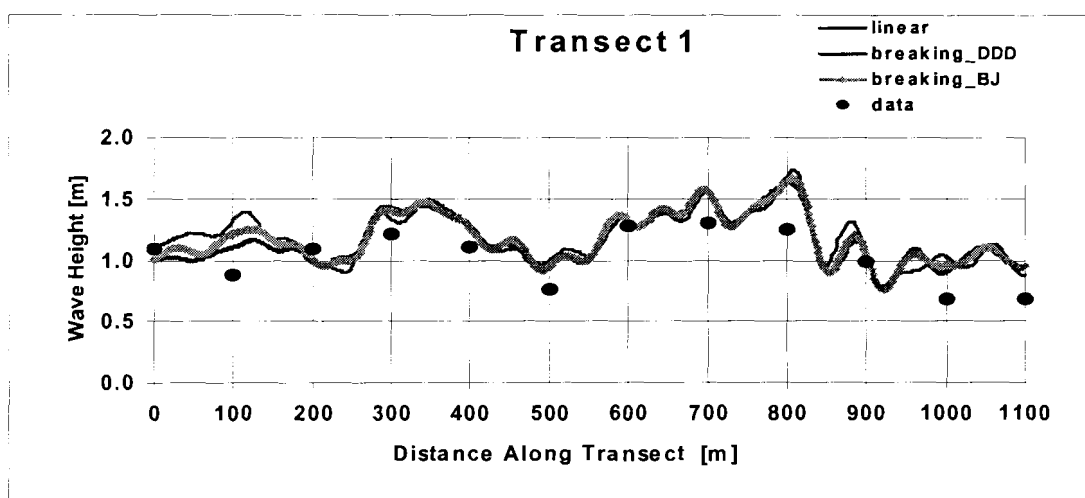


Figure 10. Wave height for Transect 1 monochromatic case 2

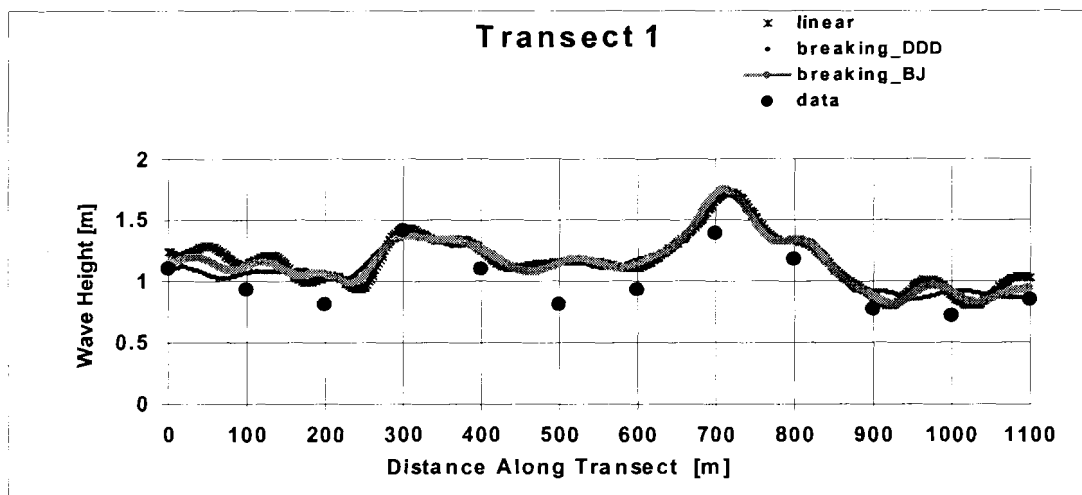


Figure 11. Wave height for Transect 1 monochromatic case 3

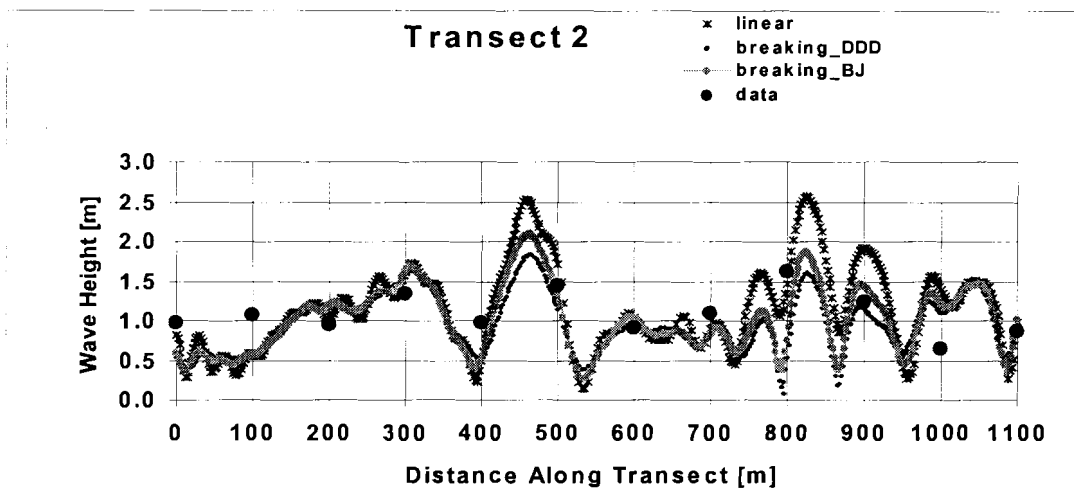


Figure 12. Wave height for Transect 2 monochromatic case 1

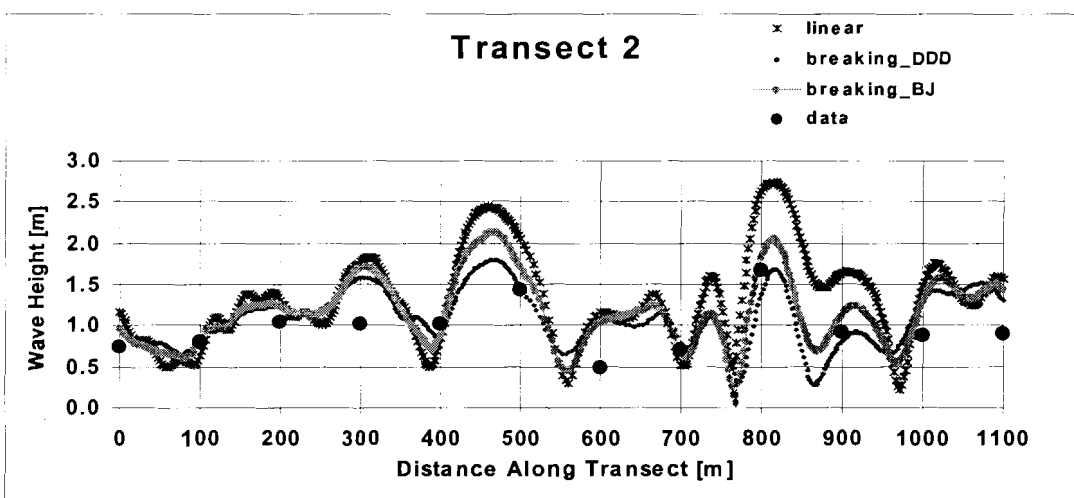


Figure 13. Wave height for Transect 2 monochromatic case 2

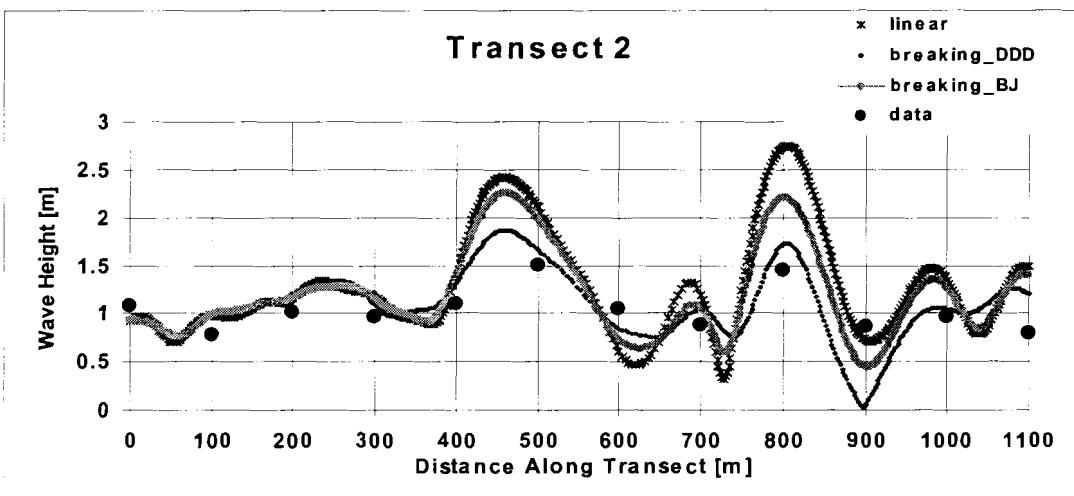


Figure 14. Wave height for Transect 2 monochromatic case 3

Table 6. RMS wave height errors for Transect 1 monochromatic cases

Transect 1					
Case Num.	Simulation Num.	Wave Period (sec.)	Incident Wave Direction (deg.)	Type (linear/ breaking)	RMS wave height errors (m)
1. (Case 1 in Table 1)	1	8	270	linear	0.222
	2	8	270	breaking (DDD)	0.204
	3	8	270	breaking (BJ)	0.215
2. (Case 2 in Table 1)	1	10	270	linear	0.268
	2	10	270	breaking (DDD)	0.214
	3	10	270	breaking (BJ)	0.232
3. (Case 3 in Table 1)	1	15	270	linear	0.197
	2	15	270	breaking (DDD)	0.214
	3	15	270	breaking (BJ)	0.216

Table 7. RMS wave height errors for Transect 2 monochromatic cases

Transect 1					
Case Num.	Simulation Num.	Wave Period (sec.)	Incident Wave Direction (deg.)	Type (linear/ breaking)	RMS wave height errors (m)
1. (Case 4 in Table 1)	1	8	270	linear	0.406
	2	8	270	breaking (DDD)	0.471
	3	8	270	breaking (BJ)	0.429
2. (Case 5 in Table 1)	1	10	270	linear	0.564
	2	10	270	breaking (DDD)	0.283
	3	10	270	breaking (BJ)	0.329
3. (Case 6 in Table 1)	1	15	270	linear	0.536
	2	15	270	breaking (DDD)	0.324
	3	15	270	breaking (BJ)	0.402

The rapid variability seen in the predictions and model data for these simulations suggests that including the “steep slope terms” in the mild-slope equation may be necessary in this application. It is of course possible to introduce dissipation or adjust reflection coefficients to tune the model for a more satisfactory agreement between the predictions and the data. A more thorough calibration of CGWAVE model was not pursued since the model performance was considered to be fair and acceptable given the uncertainties alluded to about the measurements.

5.2. Spectral Simulations

Three cases (cases 4, 5 and 6 in Table 1) were studied for the spectral simulations. These cases are also referred to as spectral cases 1, 2 and 3 in the discussion below. For each spectral case two spectral components (a higher and a lower spectral components) were created using the TMA spectra equations described in section 2.2 and 4.3. To determine if sufficient numbers of spectral components were created for each spectral case, a comparison between a lower and higher spectral component simulations was evaluated graphically and the results are discussed and shown in this section. Input and boundary conditions for each spectral case is summarized in Table 8. Also for all the spectral cases, a reflection coefficient of 0.95 was used for the jetty (i.e. nearly fully reflective structure), and 0 (fully absorbing) for the coastlines (Table 9). In all the three spectral cases two linear simulations were made to compare the results between a lower and higher component simulation for both transects. The input conditions that were used to create the spectrum are shown in Table 1 in Chapter 2. Table 8 above summarizes the frequency and directional bins used for each spectral simulation. The term “spectral

simulation” is referred to the simulations performed with the numerical model CGWAVE. For example, in Table 8 for spectral case 1 (case #4 in Table 1) three spectral simulations (1, 2 and 3) were performed with numerical model CGWAVE, two linear simulations (one with 70 spectral components and the other with 306 spectral components) and one non-linear simulation (DDD breaking simulation, with 306 spectral components). As shown in Table 8, the lower end of the frequency band is f_1 and the higher end of the frequency band is f_2 with a segment size of Δf . Similarly, the lower end of the angular band is θ_1 and the higher end of the angular band is θ_2 with a segment size of $d\theta$. In addition to the two linear spectral simulations, a non-linear simulation was made with breaking turned on, using the higher number of spectral component (306 spectral components). In all the three spectral cases only the DDD breaking case was studied. Please refer to section 4.3 for details of creating the spectrum.

Table 8. Input conditions for spectral simulations for spectral cases

Case Num.	Run Num.	Num. Comp.	Type (linear/breaking)	CGWAVE Input Conditions							
				f1 Hz	f2 Hz	fp Hz	Δf Hz	θ_1 deg	θ_2 deg	θ_m deg	$\Delta\theta$ deg
1. (Case 4 in Table 1)	1	70	linear	0.085	0.2498	0.125	0.0412	180	310	240	10
	2	306	linear	0.08	0.335	0.125	0.015	200	280	240	5
	3	306	breaking	0.08	0.335	0.125	0.015	200	280	240	5
2. (Case 5 in Table 1)	1	42	linear	0.087	.152	0.1	0.013	225	315	270	15
	2	66	linear	0.087	.152	0.1	0.013	220	320	270	10
	3	66	breaking	0.087	.152	0.1	0.013	220	320	270	10
3. (Case 6 in Table 1)	1	78	linear	0.048	0.178	0.067	0.026	270	330	300	5
	2	91	linear	0.045	0.165	0.067	0.02	270	330	300	5
	3	91	breaking	0.045	0.165	0.067	0.02	270	330	300	5

Table 9. Boundary conditions for spectral simulations for spectral cases

CGWAVE	
Boundary Conditions for spectral simulations for all three cases and simulations	
Reflection Coefficients for Coastline	Reflection Coefficients for Jetty
0.0	0.95

The following plots and tables summarize results for the spectral cases (Table 8) mentioned above. Results for CGWAVE model predictions from the spectral simulations are compared against physical model data in Figures 15, 16 and 17 for Transect 1, and in Figures 18, 19 and 20 for Transect 2. Similarly, spectral statistical numerical model estimates (RMS wave height errors) of the wave heights are presented in Table 10 for Transect 1 and Table 11 for Transect 2. Summary and discussions of the spectral results will follow the figures and statistical tables for both transects.

Both graphical and statistical results indicate that spectral simulations made with a lower number of total spectral components were not much different from those with a higher number of components for both transects. Therefore, it was concluded that spectral resolution might not be as significant a factor as it has often been assumed in other studies. This confirmed that a sufficient number of components have been used in the spectral simulations presented here. For simulations with wave breaking, only the DDD breaking formula was used in all the three simulations using the highest number of components.

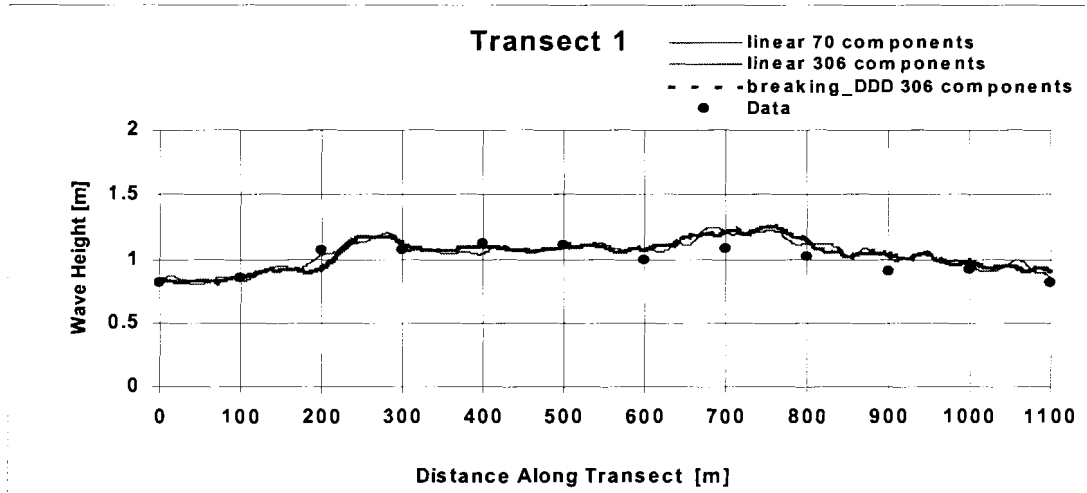


Figure 15. Wave height for Transect 1 spectral case 1 (case # 4 in Table 1)

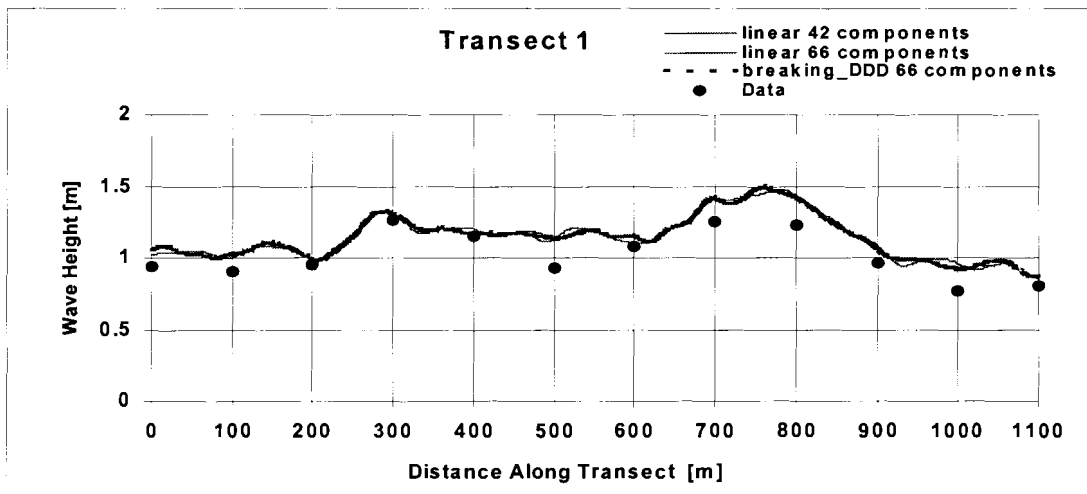


Figure 16. Wave height for Transect 1 spectral case 2 (case # 5 in Table 1)

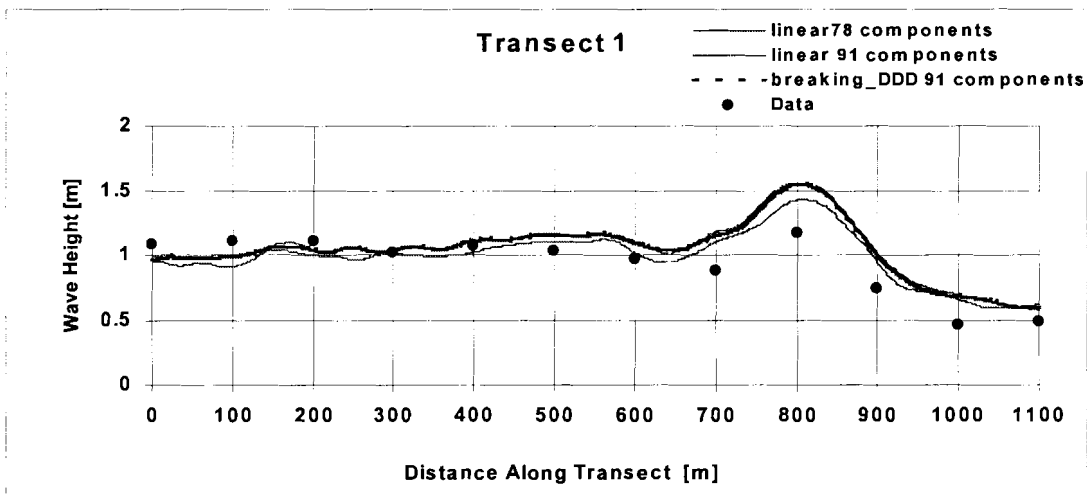


Figure 17. Wave height for Transect 1 spectral case 3 (case # 6 in Table 1)

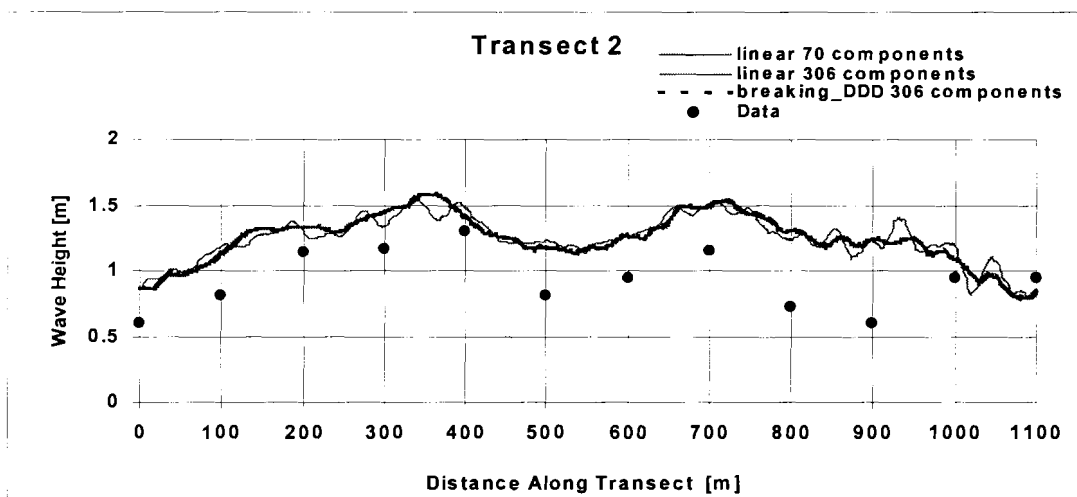


Figure 18. Wave height for Transect 2 spectral case 1 (case # 4 in Table 1)

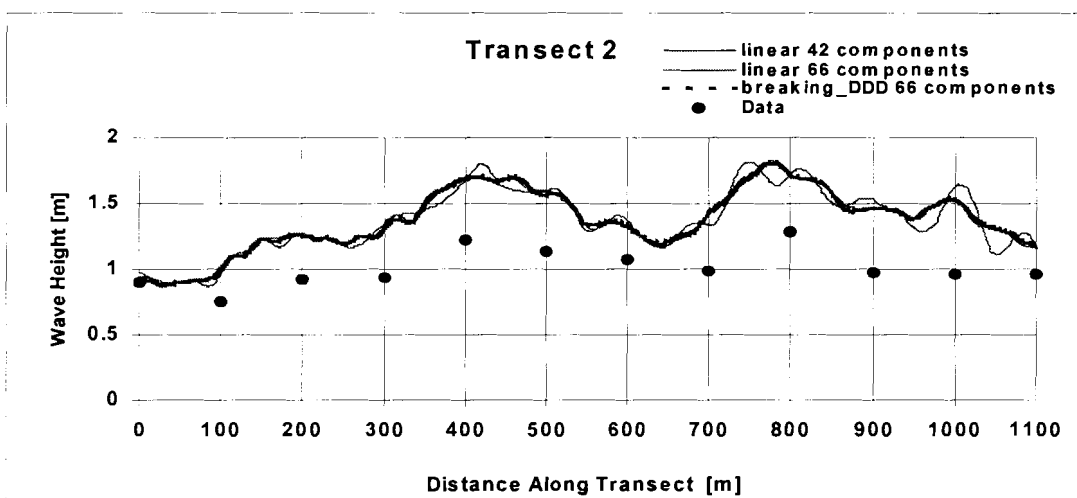


Figure 19. Wave height for Transect 2 spectral case 2 (case #5 in Table 1)

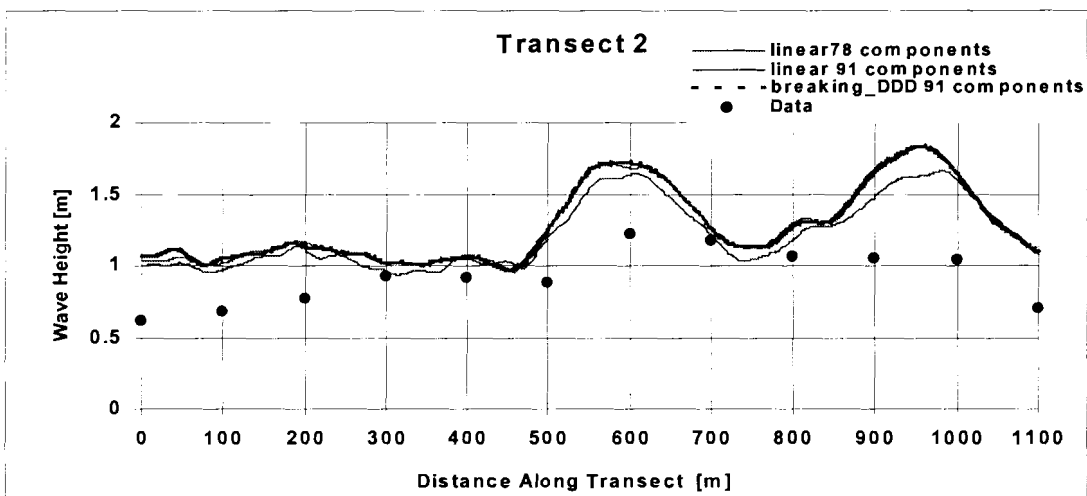


Figure 20. Wave height for Transect 2 spectral case 3 (case #6 in Table 1)

Table 10. RMS wave height errors for Transect 1 spectral cases

Transect 1				
Spectral Case Num.	Spectral Simulation Num.	Num. Comp.	Type (linear/ breaking)	RMS wave height errors (m)
1. (Case 4 in Table 1)	1	70	linear	0.139
	2	306	linear	0.141
	3	306	breaking (DDD)	0.142
2. (Case 5 in Table 1)	1	42	linear	0.240
	2	66	linear	0.142
	3	66	breaking (DDD)	0.227
3. (Case 6 in Table 1)	1	78	linear	0.280
	2	91	linear	0.322
	3	91	breaking (DDD)	0.322

Table 11. RMS wave height errors for Transect 2 spectral cases

Transect 2				
Spectral Case Num.	Spectral Simulation Num.	Num. Comp.	Type (linear/ breaking)	RMS wave height errors (m)
1. (Case 4 in Table 1)	1	70	linear	0.495
	2	306	linear	0.484
	3	306	breaking (DDD)	0.483
2. (Case 5 in Table 1)	1	42	linear	0.585
	2	66	linear	0.483
	3	66	breaking (DDD)	0.560
3. (Case 6 in Table 1)	1	78	linear	0.478
	2	91	linear	0.518
	3	91	breaking (DDD)	0.518

Unlike the monochromatic simulations, the performance of the numerical model for spectral simulations was quantified using the significant wave height estimates, since measured data for spectral runs was in the form of a significant wave. As shown graphically, for all the 3 spectral cases for both transects, the agreement between model predictions and data is considerably better compared to results for monochromatic simulations (Figures 9 to 14 for monochromatic cases and Figures 15 to 20 for spectral cases). We also note that a more satisfactory comparison is obtained at Transect 1, similar to the results for the monochromatic simulations. Possible reasons were given earlier in the monochromatic wave case section.

We should also note that wave breaking had little or no effect on spectral predictions, as it did not change any of the spectral simulation results. This is not surprising since wave breaking criteria used in these simulations were based on the wave height of the individual wave components. Since the heights of individual wave components in a spectra are usually a very small fraction of the total significant wave height representing the spectra, it is obvious that wave breaking formulas must use the significant wave height for it to be useful in practice. This would require re-writing CGWAVE model code and re-validating it from ground zero, which was not in the scope of this research. Zhao et al. (2001) have developed a version of CGWAVE that utilizes the significant wave height in wave breaking formulas. Their model could not be considered in Ponce de Leon Inlet application, as it would have demanded enormously higher computational resources.

Finally, we see that overall, spectral simulations provide much smoother results at both transects. This may be due to the combination of results for a range of wave periods and directions, and this trend has been also noted in several previous studies using other wave models Smith and Harkins (1997), Panchang et al. (1990).

Chapter 6

SUMMARY AND CONCLUSIONS

It is often necessary to implement wave models on coastal domains where there are insufficient data for validation. Results may have to be accepted at face value (without tuning.) This is difficult from the user's viewpoint; for example, see Thieler et al. (2000) who suggest that several models may demonstrate poor performance in the field. It is therefore important to demonstrate that the models provide reasonable predictions using whatever data are available. Many US Army Corps of Engineers' coastal engineering projects rely on numerical wave models to estimate wave transformation over irregular bathymetries from deep waters offshore to shallower depths in the near shore domain. To evaluate capabilities of wave models commonly used by the Corps of Engineers, a suite of wave conditions were generated in a laboratory environment and these waves were transformed over a physical model of the ebb shoal representing the bathymetry of the Ponce de Leon Inlet, Florida, USA. Measurements were made along two shore-parallel transects (Transects 1 and 2) where linear arrays of capacitance-type wave gauges were used to measure changes in wave parameters resulting from their transformation over the complex bathymetry. In this thesis, an evaluation of the numerical wave model CGWAVE using the Ponce de Leon Inlet laboratory measured data is presented.

Measured and predicted spectral and monochromatic wave heights along the offshore (Transect 1) and near shore arrays (Transect 2) are similar in general trends. It is

not surprising to see monochromatic cases have larger spatial gradients in wave height than the spectral cases. The nature of wave focusing at the near shore array is noticeably different between the spectral and monochromatic cases. Monochromatic cases generally show more wave focusing at the near shore array (Transect 2) than the offshore array (Transect 1), whereas the spectral cases show much smoother results at the near shore array due to the super positioning of focusing from a range of wave periods and directions. Similar results at Ponce De Leon Inlet using different numerical models (RCPWAVE, REF/DIF 1, and STWAVE) were also reported by (Smith and Harkins, 1997).

As mentioned earlier, the monochromatic wave results from the numerical model CGWAVE appear to exhibit a higher level of variability than the physical model data. This is more pronounced for Transect 2 (Figures 12, 13 and 14). However it may be noted that the bathymetric variations in the Ponce de Leon Inlet study and rapid changes near Transects 1 and 2 are comparable to those in the shoal studies of Berkhoff et al. (1982) and Vincent and Briggs (1989), where data were obtained at much greater resolution (approximately 5 data points per wavelength). In both shoal experiments, measurements indicated that wave height amplification factors varied from 0.2 to 2.6. It is possible, therefore, that the physical model data for Ponce de Leon Inlet (obtained at a much coarser resolution of approximately 0.66 data points per wavelength) suffers from under-sampling. The numerical results from CGWAVE show the same kind of variability as observed data in two shoal studies, suggesting that these results obtained from the numerical model CGWAVE are reasonable.

For the monochromatic cases, wave breaking tends to bring the model results closer to the physical model in many locations. In general, CGWAVE results for the monochromatic simulations with breaking turned on compare more favorably to measured data, especially for Transect 2. Comparing the statistical results between the two breaking monochromatic simulations (DDD and BJ), the DDD wave breaking formula yielded the best comparison, which is more pronounced for Transect 2, shown in Tables 6 and 7.

Spectral simulations were performed by creating an input TMA frequency spectrum and a wrapped-normal directional distribution. Three spectral simulations for each spectral case were performed, by applying CGWAVE, two linear and one breaking (with DDD formula) mode as shown in Table 8. The number of frequency and directional bins used in the discretization of wave spectra were changed to investigate the sensitivity of CGWAVE results to the total number of spectral components specified as input to the model. Each spectral simulation was repeated with two different spectral components to make sure wave spectra had adequate number of frequency and angular (wave direction) components. Model results (wave heights) indicated that spectral simulations for all three cases made with a lower number of total spectral components were not different from those obtained with a higher number of components, and therefore, it was concluded that spectral resolution may not be as significant a factor as it is often considered. This confirmed that sufficient numbers of components were used in the spectral simulations presented here.

Overall CGWAVE results for Transects 1 and 2, exhibit far less variability in spectral wave cases (e.g. Panchang et al. 1980). Also, in general, a better match between CGWAVE spectral cases estimates and measured wave height data was obtained. However, the overestimations along Transect 2 continued to persist. It should be noted that these results required no tuning of any kind, including adjustment of the coefficients used in the breaking formulations. Spectral simulations performed for Ponce de Leon Inlet confirmed that in applications when monochromatic representation of the ocean waves is inadequate for design purposes, storm waves may be simulated with CGWAVE as the superposition of individual spectral components (i.e. as monochromatic waves) insofar as nonlinear effects between frequencies are negligible.

Breaking, however, did not make any significant difference as compared to the linear simulations, in any of the spectral cases. This could be due to the fact that the breaking factor was calculated independently on the basis of individual component simulations instead of on the basis of the significant wave height (SWH). Additional breaking simulations performed by Zhao et al. (2001) have shown improvement between model and data comparison along several transects including Transect 1 and 2. Improved performance was achieved by using the significant wave height (SWH) instead of the component wave height in the breaking formulas considered here. The use of significant wave height based breaking criteria, as opposed to individual wave height of the spectral component, may be warranted since this approach has improved the model-data comparison along Transect 2. The remaining difference between model and data must be attributed to potential problems associated with the physical model and data analysis used

in that study. This model validation study can be used to guide future applications of CGWAVE model in other projects. Lessons learned in this study are summarized below:

- 1) As mentioned above, monochromatic cases generally show more wave focusing at the near-shore array (Transect 2) than the offshore array (Transect 1), whereas the spectral cases show much smoother results at the near-shore array due to the super-positioning of focusing from a range of wave periods and directions. This finding was also reported by Holthuijsen et al. (1993) and by Panchang et al. (1990).
- 2) RMS wave height errors for monochromatic and spectral cases were in the range of 0.139 m to 0.585 m for both transects while some errors are insignificant, the errors are probably due to uncertainties in the input obtained from the physical model or under-sampling. The numerical model CGWAVE reliably captured the wave height trends observed at the gauges.
- 3) Breaking did not have a significant influence on the data (i.e. decrease the RMS wave height errors or smoothen the trend plots), perhaps due to the range of the wave heights being small.
- 4) Overall, results from the numerical model CGWAVE were as representative as the lab data.

Lessons learned and knowledge gained about Ponce de Leon Inlet model performance can help users to determine the applicability of this numerical model,

CGWAVE, and thus may help to reduce the need for field or laboratory data measurements that may be costly.

REFERENCES

- Berkhoff, J. C. W. (1976). *Mathematical Models for Simple Harmonic Linear Water Waves. Wave Refraction and Diffraction*, Publ. 163, Delft Hydraulics Laboratory.
- Booij, N. (1981). *Gravity Waves on Water with Non-uniform Depth & Current*, Ph.D. thesis, Technical Univ of Delft, The Netherlands.
- Bova, S. W., C. P. Breshears, C. Cuicchi, Z. Demirbilek, and H. A. Gabb (2000). Dual-level Parallel Analysis of Harbor Wave Response Using MPI and OpenMPI. *Intl. J. High Performance Computing Applications*. v14, 1, 49-64.
- Chen, H. S. (1990). Infinite Elements for Water Wave Radiation and Scattering. *Intl. J. Numerical Methods in Fluids*. v11, 555-569.
- Chen, H. S., and J. R. Houston (1987). Calculation of Water Level Oscillations in Harbors, *Instructional Rept. CERC-87-2, Waterways Expt. Stn*, Vicksburg, Mississippi 39180.
- Chiang, W.-L. (1988). Modeling Long and Intermediate Waves in a Harbor. *Appl. Math. Modeling*. v12, 423-428.
- Dalrymple, R. A., J. T. Kirby, and P. A. Hwang (1984). Wave Diffraction due to Areas of High-energy Dissipation. *J. Waterway, Port, Coastal & Ocean Eng.* v110, 1, 67-79.
- Demirbilek, Z., and V. G. Panchang (1998). CGWAVE: A Coastal Surface Water Wave Model of the Mild Slope Equation, *Tech Rept CHL-98-26, US Army Corps of Engineers Waterways Expt Stn*, Vicksburg, Mississippi 39180.
- Dingemaans, M. W. (1997). *Water Wave Propagation over Uneven Bottoms*. World Scientific. Singapore.
- Dongcheng, Li (2002). Los Angeles-Long Beach Harbor Pier 400 Harbor Resonance Study Using Numerical Model CGWAVE.
- Ebersole, B. A. (1985). Refraction-Diffraction Model for Linear Water Wave. *J. Waterway, Port, Coastal & Ocean Eng.* v111, 6, 939-953.
- Givoli, D. (1991). Non-reflecting Boundary Conditions. *J. Computat. Physics*, 94, 1-29.
- Holthuijsen L.H., N. Booij, and R.C. Ris (1993). A Spectral Wave Model For The Coastal Zone.

- Hurdle, D. P., J. K. Kostense, and P. Bosch (1989). Mild Slope Model for the Wave Behaviour in & around Harbours and Coastal Structures. In: *Advance in Water Modeling and Measurement*. Ed. M. H. Palmer. BHRA, The Fluid Engg Centre, Cranfield, England. 307-324.
- Irons, P. (1970). A Frontal Solution Program for Finite Element Analysis. *Internatl. J. Numerical Methods Eng.* 2, 5-32.
- Isaacson, M., and S. Qu (1990). Waves in a Harbour with Partially Reflecting Boundaries. *Coastal Engg.* v14, 193-214.
- Jones, N. L., and D. R. Richards (1992). Mesh Generation for Estuarine Flow Models. *J. Waterway, Port, Coastal and Ocean Eng.* v118, No. 6, 3-20.
- Kirby, J. T. (1986). Higher Order Approximation in the Parabolic Equation Method for Water Waves. *J. Geophys. Research.* 91 (c1), 933-952.
- Kostense, J. K., K. L. Meijer, M. W. Dingemans, A. E. Mynett, and P. van den Bosch (1986). Wave Energy Dissipation in Arbitrarily Shaped Harbours of Variable Depth. *Proc. 20th Intl. Conf. Coastal Engg., Washington D. C.* 2002-2016.
- Kostense, J. K., M.W. Dingemans, and P. van den Bosch (1988). Wave-Current Interaction in Harbours. *Proc. 21st Internat. Conf. Coastal Engg., ASCE, New York*, v1, 32-46.
- Lee, J. J., and F. Raichlen (1972). Oscillations in Harbors with Connected Basins. *J. Waterways, Harbors, and Coastal Engg Div, ASCE.* v98, 311-332.
- Lennon, G. P., P. L.-F. Liu, and J. A. Liggett (1982). Boundary Integral Solutions of Water Wave Problems. *J. Hydr. Div. ASCE.* v108, 921-931.
- Li, B. (1994a). A Generalized Conjugate Gradient Model for the Mild Slope Equation. *Coastal Engg.* 23, 215-225.
- Li, B. (1994b). An Evolution Equation for Water Waves. *Coastal Engg.* 23, 227-242.
- Li, B., and K. Anastasiou (1992). Efficient Elliptic Solvers for the Mild-Slope Equation using the Multigrid Method. *Coastal Engg.* 16, 245-266.
- Li, B., D. E. Reeve, and C. A. Fleming (1993). Numerical Solution of the Elliptic Mild-Slope Equation for Irregular Wave Propagation. *Coastal Engg.* 20, 85-100.
- Mei, C. C. (1983). *The Applied Dynamics of Ocean Surface Waves*. John Wiley, New York.

- OARB (1997). OpenMP Fortran Application Program Interface. *OpenMP Architecture Review Board (OARB) v1.0*, <http://www.openmp.org>, October 1997.
- Oliveira, F. S. B. F., and K. Anastasiou (1998). An Efficient Computational Model for Water Wave Propagation in Coastal Regions. *Applied Ocean Research*, 20, 3, 263-271.
- Panchang, V. G., B. Cushman-Roisin, and B. R. Pearce (1988). Combined Refraction-Diffraction of Short Waves for Large Coastal Regions. *Coastal Engg.* v12, 133-156.
- Panchang V. G., G. Wei, B. R. Pearce, and M. J. Briggs (1990). Numerical Simulations of Irregular Wave Propagation Over Shoal. *J. Waterway, Port, Coastal, & Ocean Engineering* V116, 3, 324-340
- Panchang, V. G., W. Ge, B. Cushman-Roisin, and B. R. Pearce (1991). Solution to the Mild-Slope Wave Problem by Iteration. *Applied Ocean Research*. 13, 4, 187-199.
- Panchang, V. G., B. Xu, and B. Cushman-Roisin. (1993). Bathymetric Variations in the Exterior Domain of a Harbor Wave Model, Proc. *Internat. Conf. on Hydroscience & Engineering, Washington D.C.* 1555-1562.
- Panchang, V. G., B. Xu, and Z. Demirbilek (1999). Wave Prediction Models for Coastal Engineering Applications. Ch. 4 in: *Developments in Offshore Engineering*, Ed. J. B. Herbich. Gulf Publishing, Houston. 163-194.
- Panchang, V. G., W. Chen, B. Xu, K. Schlenker, Z. Demirbilek, and M. Okihiro (2000). Effects of Exterior Bathymetry in Elliptic Harbor Wave Models, *J. Waterway, Port, Coastal & Ocean Engg.* v126, 2, 71-78.
- Panchang, V. G., and Z. Demirbilek (2001). Simulation of Waves in Harbors using Two-Dimensional Elliptic Equation Models. *Advances in Coastal and Ocean Engg.* v7., 125-162.
- Pos, J. D., and F. A. Kilner (1987). Breakwater Gap Wave Diffraction: An Experimental and Numerical Study. *J. Waterway, Port, Coastal, & Ocean Engg.*, v113, 1, 1-21.
- Radder, A. C. (1979). On the Parabolic Equation Method for Water-Wave Propagation. *J. Fluid Mech.* 95, 159-176.
- Schaffer, H. A., and I. G. Jonsson (1992). Edge Waves Revisited. *Coastal Engg.*, v16, 349-368.

- Seabergh, W. C., and L. J. Thomas (1995). Los Angeles Harbor Pier 400 Harbor Resonance Model Study. US Army Corps of Engineers Waterways Expt Stn, Vicksburg, MS 39180. TR CERC-95-8.
- Smith, G. D. (1978). Numerical Solution of Partial Differential Equations: Finite Difference Methods. Oxford University Press, Oxford.
- Smith, R., and T. Sprinks (1975). Scattering of Surface Waves by a Conical Island. *J. Fluid Mech.* 72, 373.
- Smith, S. J., and G. Harkins, (1997) Numerical Wave Model Evaluations using Laboratory data, *Proc. Waves'97, ASCE*, 271-285.
- Thompson, E. F., H. S. Chen, and L. L. Hadley (1996). Validation of Numerical Model for Wind Waves and Swell in Harbors. *J. Waterway, Port, Coastal and Ocean Engg.* v122, 5, 245-256.
- Tsay, T.-K., and P. L.-F. Liu (1983). A Finite Element Model for Wave Refraction and Diffraction. *Applied Ocean Research* v5, 1, 30-37.
- Tsay, T.-K., W. Zhu, and P. L.-F. Liu (1989). A Finite-Element Model for Wave Refraction, Diffraction, Reflection, and Dissipation. *Applied Ocean Research.* 11, 33-38.
- Xu, B., and V. G. Panchang (1993). Outgoing Boundary Conditions for Elliptic Water Wave Models. *Proceedings, The Royal Society of London, Series A.* v441, 575-588.
- Xu, B., V. G. Panchang, and Z. Demirbilek (1996). Exterior Reflections in Elliptic Harbor Wave Models. *J. Waterway, Port, Coastal and Ocean Engg.* v122, 3, 118-126.
- YOTO (1998). "Our Ocean Future," Year of the Ocean, Themes & Issues Concerning the Nation's Stake in the Oceans. Prepared by the H. John Heinz III Center for Science, Economics, and the Environment. Office of the Chief Scientist, NOAA, Washington, DC 20230.

- Zhao L., V. G. Panchang, W. Chen, Z. Demirbilek, and N. Chhabra (2001). Simulation of Wave Breaking Effects in Two-dimensional Elliptic Harbor Wave Models. *Coastal Engineering*. 42, 359-373.
- Zundel, A. K., A. L. Fugal, N. L. Jones, and Z. Demirbilek (1998). Automatic Definition of Two-dimensional Coastal Finite Element Domains. In: *Hydroinformatics98, Proc. 3rd Internat. Conf. Hydroinformatics*. Ed. V. Babovic and L. C. Larsen. A. A. Balkema, Rotterdam. 693-700.

BIOGRAPHY OF THE AUTHOR

Nishchey Chhabra was born in Paisley, Scotland, UK on August 26, 1971. He moved to Shiraz, Iran in 1979 where he attended the Shiraz International Community School till 6th grade. He then moved to Gwalior, India where he completed his 7th grade at Scindia school. He graduated high school from Gujarat Law Society school at Ahmedabad, India in 1990.

In August 1990, Nishchey entered Dayananda Sagar Institute of Technology (DSIT) and in June 1993 he received his Diploma in Mechanical Engineering degree.

Nishchey enrolled as an undergraduate in Mechanical Engineering in the fall of 1993 at the University of Maine in Orono, Maine. He received his Bachelor of Science in Mechanical Engineering degree in the fall of 1996. He then continued in the master's program in Mechanical Engineering in the spring of 1997.

In December 1998 Nishchey accepted a contract position at the General Electric Company as a test engineer in Schenectady, New York. In January 2001 Nishchey accepted a full time position with the General Electric Company as a Systems Test Engineer and moved to Greenville, South Carolina where he currently resides. Nishchey is a candidate for the Master of Science degree in Mechanical Engineering from The University of Maine in May, 2004.